

Article

A balance between antagonizing PAR proteins specifies the pattern of asymmetric and symmetric divisions in *C. elegans* embryogenesis

Yen Wei Lim,^{1,2} Fu-Lai Wen,^{3,6} Prabhat Shankar,^{3,6} Tatsuo Shibata,^{3,*} and Fumio Motegi^{1,2,4,5,7,*}

¹Temasek Life-sciences Laboratory, Singapore 117604, Singapore

²Department of Biological Sciences, National University of Singapore, Singapore 117583, Singapore

³RIKEN Center for Biosystems Dynamics Research, Kobe 650-0047, Japan

⁴Mechanobiology Institute, National University of Singapore, Singapore 117411, Singapore

⁵Institute for Genetic Medicine, Hokkaido University, Sapporo 060-0815, Japan

⁶These authors contributed equally

⁷Lead contact

*Correspondence: tatsuo.shibata@riken.jp (T.S.), motegi@igm.hokudai.ac.jp (F.M.)

<https://doi.org/10.1016/j.celrep.2021.109326>

SUMMARY

Coordination between cell differentiation and proliferation during development requires the balance between asymmetric and symmetric modes of cell division. However, the cellular intrinsic cue underlying the choice between these two division modes remains elusive. Here, we show evidence in *Caenorhabditis elegans* that the invariant lineage of the division modes is specified by the balance between antagonizing complexes of partitioning-defective (PAR) proteins. By uncoupling unequal inheritance of PAR proteins from that of fate determinants during cell division, we demonstrate that changes in the balance between PAR-2 and PAR-6 can be sufficient to re-program the division modes from symmetric to asymmetric and vice versa in two daughter cells. The division mode adopted occurs independently of asymmetry in cytoplasmic fate determinants, cell-size asymmetry, and cell-cycle asynchrony between sister cells. We propose that the balance between PAR proteins represents an intrinsic self-organizing cue for the specification of the two division modes during development.

INTRODUCTION

The development of a multicellular organism requires strict control of the balance between cell proliferation and differentiation. Within a developing embryo, each cell proliferates by either the asymmetric or symmetric mode of cell division (Horvitz and Herskowitz, 1992), yielding two daughter cells with either distinct or identical cellular constituents, respectively. The symmetric mode of cell division gives rise to two copies of the mother cell. The asymmetric mode of cell division results in unequal inheritance of fate determinants, which will promote the subsequent induction of distinct cellular fates between the daughter cells. Asymmetric cell division can be accompanied by differences in cell size between the two daughter cells. The balance between the two modes of cell division is controlled during embryogenesis as well as during postnatal development. Many adult stem cells exhibit the homeostatic control of self-renewal and differentiation by balancing the two modes of cell division (Chen et al., 2016; Knoblich, 2008). Disruption of this balance results in developmental disorders, premature depletion of the stem cells, and abnormal growth of prenatal and postnatal organs.

The specification between asymmetric and symmetric modes of cell division is mediated by an intrinsic program (i.e., cell-

autonomous manner) and by extrinsic stimuli that influence the intrinsic program (i.e., non-cell-autonomous manner). The resultant choice of the intrinsic cell-division program can dictate the distribution of cell-polarity regulators, which patterns the spatial organization of the entire cell (Morrison and Kimble, 2006). Therefore, these cell-polarity regulators have been considered as downstream effectors of the intrinsic cell-division program. To date, many machineries have been deemed essential for either the symmetric or asymmetric mode of cell division. However, it has been challenging to obtain rigorous data identifying the nature of the intrinsic program used to impose the choice between the two division modes. Indeed, many arguments in support of an apparent intrinsic program have relied on circumstantial evidence, such as a combination of the mother cell polarity, inhomogeneity of external environment, and unequally sized daughter cells. Thus, the identity of the cue that dictates the intrinsic cell-division program is not completely understood.

We investigated the intrinsic program underlying the specification between asymmetric and symmetric modes of cell division by using the developing *Caenorhabditis elegans* embryo, which has an invariant lineage (Sulston and Horvitz, 1977; Sulston et al., 1983), as a model system. The newly fertilized *C. elegans* zygote undergoes asymmetric cell division in a cell-autonomous



manner, yielding two daughter cells, namely, AB and P1 (Figure S1A). During the first cell division, the inner layer of the plasma membrane (i.e., the cell cortex) is compartmentalized by segregation of the cell-polarity regulators partitioning-defective (PAR) proteins (Goldstein and Macara, 2007; Kemphues, 2000). PAR-3, PAR-6, atypical protein kinase C (aPKC), and the active form of CDC-42 GTPase become enriched at the anterior cortex (Etemad-Moghadam et al., 1995; Hung and Kemphues, 1999; Tabuse et al., 1998), whereas PAR-1 and PAR-2 localize at the posterior cortex (Boyd et al., 1996; Guo and Kemphues, 1995; Figure S1A). It has been widely accepted that cortical patterning of PAR proteins is largely attributed to the principle of mutual inhibition, wherein proteins from one cortical domain antagonize the co-localization of proteins from the other domain and vice versa (Hoege and Hyman, 2013). The spatially biased distribution of PAR proteins is essential to segregate cytoplasmic fate determinants (e.g., MEX-5, PIE-1, and P-granules) and displace the mitotic spindle toward the posterior pole. Consequently, the two daughter cells comprise distinct concentration of fate determinants, cell-size asymmetry, and cell-cycle asynchrony (Griffin, 2015; Rose and Gonczy, 2014; Figure S1A). Displacement of the mitotic spindle and the consequent asymmetry in cell size are not necessary for the unequal inheritance of fate determinants (Gotta and Ahringer, 2001; Gotta et al., 2003). In this study, asymmetric and symmetric modes of cell division were defined as the cellular ability to accomplish asymmetric segregation and unequal inheritance of both PAR proteins and fate determinants during mitosis.

The above-described cell polarity cascade in zygotes programs the two daughter cells AB and P1 to undergo symmetric and asymmetric cell division, respectively. During the second cell division, the polarized distributions of cortical PAR proteins and the cytoplasmic fate determinants are reiterated only in P1 cells but not in AB cells (Figure S1A). This commitment of AB and P1 cells to their respective mode of cell division occurs in a cell-autonomous manner (Priess and Thomson, 1987), indicating that the cue that dictates to the intrinsic cell-division program must be unequally inherited during the first cell division. AB and P1 cells also acquire differential abilities regarding the rotation of mitotic spindles. The AB spindle remains orthogonal to the anteroposterior axis, whereas the P1 spindle is rotated and aligned with the axis. This rotation of mitotic spindles depends on a combination of cell-autonomous manner (Cheng et al., 1995; Kemphues et al., 1988; Kotak, 2019) and non-cell-autonomous manner (Singh and Pohl, 2014; Sugioka and Bowerman, 2018). Still, the identity of the cue dictating the choice between symmetric and asymmetric modes of cell division in AB and P1 cells remains unclear.

In this report, we developed experimental systems that enabled the independent assessment of the roles of PAR proteins and the asymmetry of fate determinants, cell size, and cell-cycle progression in two-cell-stage embryos. Using genetic manipulations that uncoupled the inheritance of PAR proteins from that of the fate determinants during the first cell division, we demonstrate that changes in the balance between antagonizing PAR proteins can be sufficient to re-program the cell division mode from symmetric to asymmetric and vice versa in two-cell-stage embryos. Specification of the division mode occurs independently of the unequal inheritance of fate determinants, cell-size asymmetry, and cell-cycle asynchrony between the sis-

ter cells. Therefore, we propose that the balance between PAR proteins represents an intrinsic self-organizing cue for the specification regarding the two division modes.

RESULTS

Genetic manipulation of PAR protein inheritance during the first cell division

This study aimed to investigate the functions of PAR proteins in the specification between asymmetric and symmetric modes of cell division in AB and P1 cells of two-cell-stage *C. elegans* embryos. Because transcriptional and translational regulation generally remain quiescent from the one-cell- to the two-cell-stage embryos (Seydoux and Dunn, 1997; Seydoux et al., 1996), conventional transgene-based approaches cannot be used for efficient induction and/or depletion of PAR proteins from the onset of the second cell division. We instead sought to change the amount of PAR proteins in AB and P1 cells by manipulating asymmetric inheritance of PAR proteins during the first cell division. The prevailing model of PAR protein patterning involves reciprocal exclusion at the cortex, wherein the cortical concentration of each protein is determined by the spatially biased rates of cortical association and disassociation in the respective domains (Blanchoud et al., 2015; Cuenca et al., 2003; Dawes and Munro, 2011; Goehring et al., 2011; Hoege and Hyman, 2013). The expansion of one cortical PAR domain is antagonized not only by the opposing PAR proteins but also by a limiting pool of maternally supplied PAR proteins (Goehring et al., 2011). We thus modified the levels of specific PAR proteins in zygotes by altering the corresponding maternal supplies.

We first manipulated the maternal supplies of PAR-2 and PAR-6 by transgene expressions in the germline. The germline expression of GFP::PAR-2 rescued the polarized distribution of mCherry::PAR-6 in *par-2(ok1723)* zygotes from which endogenous *par-2* had been deleted (Figures 1A and 1B). The germline expression of mCherry::PAR-6 restored the polarized localization of GFP::PAR-2 in *par-6(3' UTR RNAi)* zygotes (Figure S1B). The germline levels of GFP::PAR-2 were modified by adapting the codon use in the *gfp::par-2* transgene (Goehring et al., 2011; Redemann et al., 2014). A stepwise increase in the transgene codon-adaptation-index (CAI) from 0.26 to 0.60 resulted in a progressive increase in the cytoplasmic intensities of GFP::PAR-2 in zygotes (Figure S1C). Consistent with a previous report (Goehring et al., 2011), zygotes overexpressing *gfp::par-2* transgenes exhibited enlarged posterior PAR-2 domains compared with the zygotes expressing unmodified GFP::PAR-2 (Figures 1A (v–viii) and 1C). These enlarged posterior PAR-2 domains were restored to a normal size by the co-expression of mCherry::PAR-6 (Figures 1A (ix–xii) and 1C). The results indicate that changes in the balance between two PAR proteins, namely, PAR-2 and PAR-6, are sufficient to alter the size of the cortical PAR domains. We then established a set of stable transgenic animals expressing various combinations of *gfp::par-2* transgenes (in the *par-2(ok1723)* background) and *mCherry::par-6* transgene (in the presence of endogenous *par-6*). These transgenes were combined with an additional genetic mutation, either *lgl-1(dd21)* or *nos-3(q650)*, which increases or reduces,

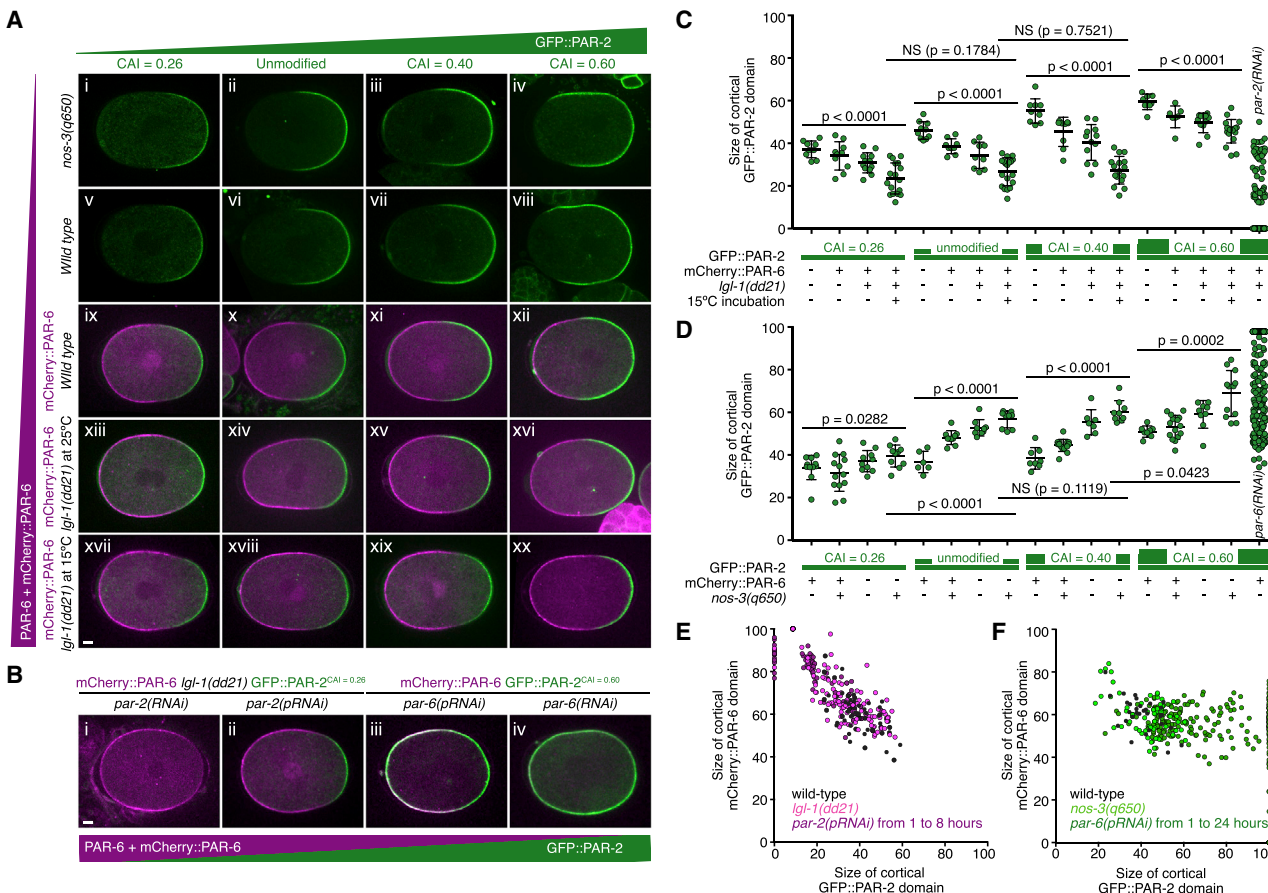


Figure 1. The landscape of PAR polarity patterning in *C. elegans* zygotes

(A) A balance between PAR-2 and PAR-6 levels defines the cortical pattern of PAR proteins in zygotes. PAR-2 levels were modified by means of *gfp::par-2* transgene codon adaptation (codon-adaptation index [CAI] values from 0.26 (i, v, ix, xiii, xvii), unmodified (ii, vi, x, xiv, xviii), 0.40 (iii, vii, xi, xv, xix), to 0.60 (iv, viii, xii, xvi, xx)) and of temperature (either at 25°C (i–xvi) or at 15°C (xvii–xx)). PAR-6 levels were changed by means of *mCherry::par-6* (green) and *nos-3(q650)* (i–iv) or *lgl-1(dd21)* (xiii–xx). Representative images of GFP::PAR-2 (green) and mCherry::PAR-6 (magenta) in live zygotes during the maintenance phase are shown. All zygotes and embryos are oriented with the posterior to the right in this and all subsequent figures. Scale bar, 5 μm.

(B) Defining the limit of PAR protein segregation. Representative images of GFP::PAR-2 (green) and mCherry::PAR-6 (magenta) in live zygotes under *par-2(RNAi)* (i) and *par-2(pRNAi)* (ii) conditions wherein PAR-6 was predominant (using MOT119 strain) (ii) and those under *par-6(pRNAi)* (iii) and *par-6(RNAi)* (iv) are shown. Scale bar, 5 μm.

(C and D) The graphs depict the size of GFP::PAR-2 cortical domains in live zygotes with various PAR balances. Height of green bars indicates the *gfp::par-2* transgene CAI. (C) Data represent mean ± SD from n = 9, 10, 12, 17, 10, 9, 9, 19, 9, 9, 12, 16, 8, 7, 11, 19, and 98 zygotes, from left to right. (D) Data represent mean ± SD from n = 9, 11, 8, 8, 4, 8, 7, 7, 6, 13, 5, 7, 6, 13, 7, 10, and 194 zygotes, from left to right. p values; Mann-Whitney test.

(E and F) The sizes of mCherry::PAR-6 and GFP::PAR-2 cortical domains in live zygotes with various balances of PAR proteins. Black circles indicate zygotes on wild-type background. Light purple (E) and light green (F) indicate zygotes on *lgl-1(dd21)* and *nos-3(q650)* backgrounds, respectively. Dark purple (E) and dark green (F) denote zygotes subjected to *par-2(pRNAi)* and *par-6(pRNAi)* treatments, respectively.

respectively, the germline level of endogenous PAR-6 (Beatty et al., 2010; Hoege et al., 2010; Pacquelet et al., 2008; Figure 1A (i–iv, xiii–xx)). We then measured the sizes of the anterior cortical mCherry::PAR-6 domain and the posterior cortical GFP::PAR-2 domain at the steady state.

We first examined the spatial patterns of cortical PAR domains in zygotes with a predominance of PAR-6. A stepwise reduction in the level of GFP::PAR-2 led to a progressive decrease in the size of the posterior PAR-2 domain (Figures 1A and 1C) without an overlap between the GFP::PAR-2 and mCherry::PAR-6 domains (Figure S1D), indicating a reciprocal increase in the size of the anterior PAR-6 domain. The various sizes of the cortical

PAR domains were converted to a consistent size (82% and 18% of the mCherry::PAR-6 and GFP::PAR-2 domains, respectively) by applying the same genetic treatment that enabled the predominance of PAR-6 (i.e., simultaneous increase in PAR-6 by *mCherry::PAR-6* expression) and the *lgl-1(dd21)* mutation and decrease in GFP::PAR-2 levels at 15°C (Figures 1A (xvii–xx) and 1C). Any further reduction in the GFP::PAR-2 levels by partial *par-2(RNAi)* [*par-2(pRNAi)*] led to the disappearance of the GFP::PAR-2 domain from the posterior cortex (Figures 1B (i, ii), 1C, 1E, S1F, and S1H). These observations suggest that the minimum size of the cortical PAR-2 domain can be maintained by a threshold. Especially, the establishment of the

posterior PAR domain exhibits a bifurcation-like feature, wherein the polarized state (i.e., the co-existent polarized PAR-6 and PAR-2 domains) can abruptly shift to an unpolarized state (i.e., homogeneous PAR-6 domain and no PAR-2 domain) if the posterior PAR domain size falls below the threshold.

We next applied a stepwise increase in the GFP::PAR-2 levels and reduction in the PAR-6 levels to yield zygotes in which PAR-2 is predominant. Remarkably, a simultaneous increase in GFP::PAR-2 expression and decrease in PAR-6 levels by *par-6(pRNAi)* caused the distribution of GFP::PAR-2 to extend into the anterior cortex, whereas mCherry::PAR-6 remained significantly enriched (Figures 1A (viii), 1B (iii), 1D, 1F, S1E, S1G, and S1I). A live-imaging analysis revealed that the boundary of the cortical mCherry::PAR-6 domain co-migrated with the posterior-to-anterior movement of cortical ruffling, whereas GFP::PAR-2 was seen throughout the cortex (Figures S2C, S2F, and S3). In zygotes expressing endogenous PAR-6 tagged with mKate2 with a moderate level of GFP::PAR-2 (CAI = 0.41), we also observed the uniform cortical distribution of GFP::PAR-2 with PAR-6::mKate2 polarized at the anterior cortical domain (Figure S1J), indicating that the cortical overlap between PAR-2 and PAR-6 does not necessarily require mCherry::PAR-6 and the highest level of GFP::PAR-2. These results indicate that the PAR system appears to permit the co-existence of an anteriorly polarized PAR-6 domain with a PAR-2 domain throughout the cortex. This violation of the reciprocal exclusion between the anterior and the posterior PAR domains cannot be explained by the conventional models of cortical PAR patterning, wherein the anterior group of proteins (PAR-3, PAR-6, PKC-3, and CDC-42) and the posterior group of proteins (PAR-1 and PAR-2) are segregated at the cortex throughout the polarization processes (Blanchoud et al., 2015; Dawes and Munro, 2011; Goehring et al., 2011).

Cortical PAR patterning by a combinatorial network between the PAR complexes and CHIN-1

To understand how PAR-6 remains polarized in the absence of reciprocal exclusion with PAR-2, we investigated the distributions of other PAR proteins in zygotes with a PAR-2 predominance. Although the polarized mCherry::PAR-6 domain was maintained, both GFP::PAR-2 and endogenous PAR-1 were localized throughout the cortex (Figures 2A (i–iv), 2B–2D, and S3A). In contrast to control zygotes, endogenous PAR-3 was significantly minimized or was undetectable at the anterior cortex (Figures 2A (v–viii), 2E, and S3B), suggesting that the polarized state of PAR-6 might be maintained independently of cortical PAR-3 concentration. PAR-3 has been considered a scaffold that locally recruits PAR-6 and PKC-3 to the active form of CDC-42 (Rodriguez et al., 2017; Wang et al., 2017). Despite the essential functions of PAR-3 in wild-type zygotes, PAR-3 becomes dispensable for the cortical loading of PAR-6 and PKC-3 in zygotes depleted of the Hsp90 co-chaperone CDC-37 (Beers and Kemphues, 2006), suggesting an alternative scaffold for PAR-6 and PKC-3. Because PAR-6 contains a CRIB domain that directly associates with the active form of CDC-42 (Aceto et al., 2006; Joberty et al., 2000), we hypothesized that active CDC-42 recruits PAR-6 directly to the anterior cortex in a manner independent on both cortical PAR-3 loading and antagonism between PAR-2 and PAR-6. To test this hypothesis, we altered the asymmetric distribution of

active CDC-42 by depleting the CDC-42 GTPase-activating protein CHIN-1. CHIN-1 localizes at the posterior cortex independently of other posterior PAR proteins and restricts CDC-42 activation only at the anterior cortex (Kumfer et al., 2010; Sailer et al., 2015). In this study, the depletion of CHIN-1 from PAR-2-predominant zygotes did not affect the initial segregation of mCherry::PAR-6 toward the anterior cortical domain (Figure S3C). However, these zygotes failed to maintain the anteriorly enriched mCherry::PAR-6 domain after the cessation of cortical flows (Figures 2F, 2G, and S3C). Consistent with the role of CDC-42 in the maintenance of the polarized PAR-6 domain, the depletion of CDC-42 blocked the polarized distribution of mCherry::PAR-6 in PAR-2-predominant zygotes (Figure S3D). Therefore, we conclude that the polarized state of PAR-6 is maintained by the accumulation of active CDC-42 at the anterior cortex through a process mediated by CHIN-1.

The conventional model of the PAR protein network includes a reciprocal exclusion pathway involving PAR-3-PKC-3-PAR-6-CDC-42 at the anterior cortex and PAR-1-PAR-2 at the posterior cortex (Blanchoud et al., 2015; Dawes and Munro, 2011; Goehring et al., 2011; Gross et al., 2019). A recent study proposed a network comprising PAR-3-PKC-3-PAR-6-CDC-42 at the anterior cortex and PAR-1-PAR-2 and CHIN-1 at the posterior cortex (Sailer et al., 2015). These models assumed that PAR-3 is essential for the local recruitment and maintenance of PAR-6 at the anterior cortex (Blanchoud et al., 2015; Dawes and Munro, 2011; Goehring et al., 2011; Gross et al., 2019; Sailer et al., 2015) and therefore cannot explain the maintenance of the polarized PAR-6 domain even at a significantly low concentration of cortical PAR-3.

Simulation of a revised model of PAR patterning in zygotes

Our results suggest that the polarized cortical PAR domains can be maintained by a cross-inhibitory network, in which the anterior cortical domain contains two species, namely, A₁ [CDC-42-PAR-6-PKC-3] and A₂ [PAR-3-PAR-6-PKC-3], and the posterior cortical domain includes two species, namely, P₁ [CHIN-1] and P₂ [PAR-1-PAR-2] (Figure 3A). To test if the cross-inhibitory network would sufficiently explain the PAR patterning in zygotes with manipulated PAR balances, we developed a mathematical model of the cross-inhibitory network. We included the following four inhibitory interactions: from A₁ [CDC-42-PAR-6-PKC-3] to P₂ [PAR-1-PAR-2], from P₂ [PAR-1-PAR-2] to A₂ [PAR-3-PAR-6-PKC-3], from A₁ [CDC-42-PAR-6-PKC-3] to P₁ [CHIN-1], and from P₁ [CHIN-1] to A₁ [CDC-42-PAR-6-PKC-3] (Figure 3A). As PAR-3 facilitates the cortical loading of PAR-6-PKC-3 during the establishment phase, we also included a positive interaction from A₂ [PAR-3-PAR-6-PKC-3] to A₁ [CDC-42-PAR-6-PKC-3] (Figure 3A). As a result, a cross-inhibitory network of PAR proteins containing PAR-3-PAR-6-PKC-3, CDC-42-PAR-6-PKC-3, and PAR-1-PAR-2 is complemented by another cross-inhibitory network involving CDC-42-PAR-6-PKC-3 and CHIN-1 (Figure 3A). A steady-state analysis of the four PAR species in a wild-type condition revealed the enrichment of A₁ [CDC-42-PAR-6-PKC-3] and A₂ [PAR-3-PAR-6-PKC-3] at the anterior cortex and that of P₁ [CHIN-1] and P₂ [PAR-1-PAR-2] at the posterior cortex (Figure 3B). Model parameter spaces for A₁ and P₂ species were defined by a previous study (Goehring et al., 2011), and those for A₂ and P₁ species were estimated by

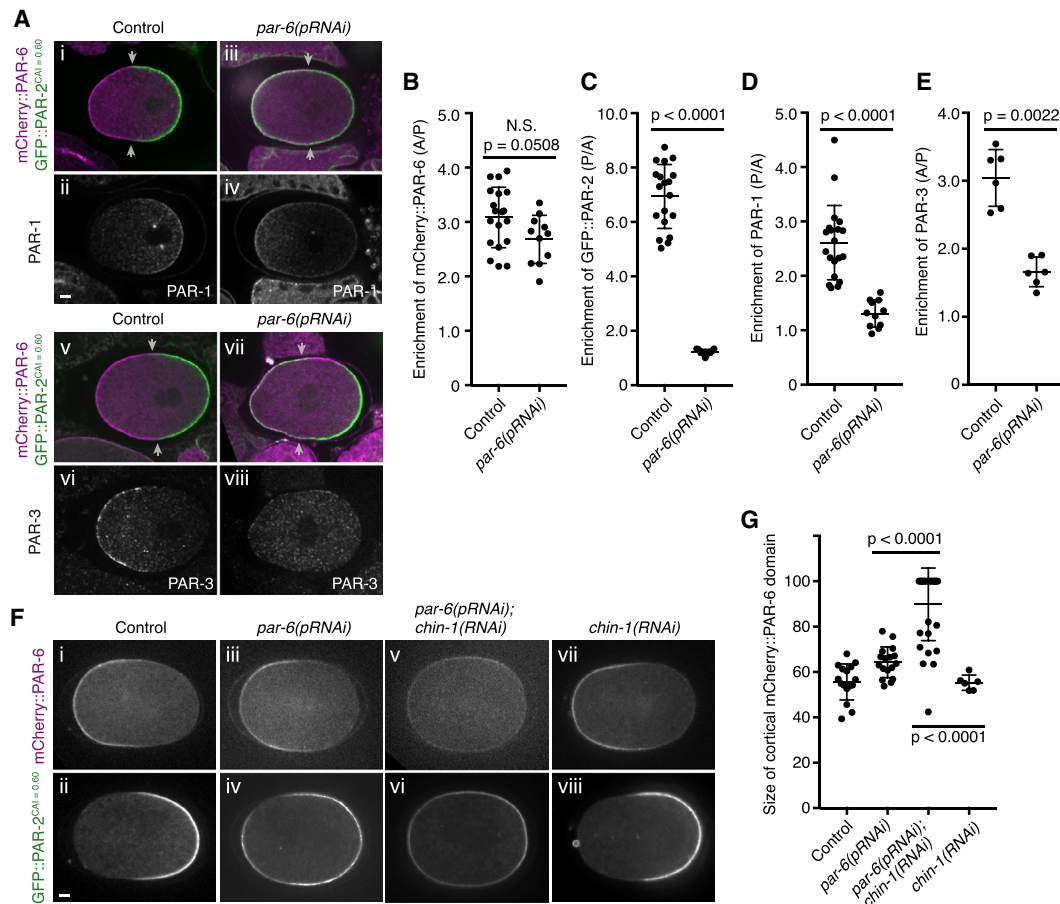


Figure 2. PAR patterning by a combinatorial network between the PAR complexes and CHIN-1

(A) The polarized distribution of PAR-3 is not required for the maintenance of the polarized PAR-6 domain. Representative immunostaining images of mCherry::PAR-6 (magenta) and GFP::PAR-2 (green) (i, iii, v, viii), PAR-1 (ii, iv), and PAR-3 (vi, viii) in control zygotes (using MOT120 strain) (i, ii, v, vi) and *par-6(pRNAi)* zygotes wherein PAR-2 was predominant (using MOT120 strain) (iii, iv, vii, viii) are shown. Arrowheads show the edges of the mCherry::PAR-6 cortical domain. Scale bar, 5 μ m.

(B–E) The graphs depict the ratios of the cortical distribution of mCherry::PAR-6 (B), GFP::PAR-2 (C), PAR-1 (D), and PAR-3 (E) between the anterior and the posterior cortical domains in control and *par-6(pRNAi)* zygotes wherein PAR-2 was predominant (using MOT120 strain). Data present mean \pm SD from n = 19, 11, 19, 11, 20, 11, 6, and 6 zygotes, from left to right.

(F) CHIN-1 is essential for the cortical polarization of PAR-6 in zygotes in which PAR-2 is predominant. Representative live zygote images of mCherry::PAR-6 (i, iii, viii) and GFP::PAR-2 (ii, iv, vi, viii) under control (i, ii), *par-6(pRNAi)* (iii, iv), *par-6(pRNAi); chin-1(RNAi)* (v, vi), and *chin-1(RNAi)* (vii, viii) conditions (using MOT120 strain) are shown. *chin-1(RNAi)* caused depolarization of mCherry::PAR-6, resulting in the weak enrichment of mCherry::PAR-6 throughout the cortex. Scale bar, 5 μ m.

(G) The graph shows the size of cortical mCherry::PAR-6 domain in zygotes under conditions shown in (F). Data present mean \pm SD from n = 16, 17, 30, and 6 zygotes, from left to right.

(B–E and G) p values; Mann-Whitney test.

searching regions that give rise to the polarized steady state in the wild-type condition (Figure S4H; Table S1). Subsequent simulation wherein the concentration of A₁ [CDC-42-PAR-6-PKC-3] (Figure 3C), P₂ [PAR-1-PAR-2] (Figure 3D), or P₁ [CHIN-1] (Figure 3E) were reduced to zero reproduced the PAR patterns observed in zygotes where either PAR-6, PAR-2, or CHIN-1 had been depleted by RNAi (Figures 3C–3E). Therefore, this model confirms the essential roles of PAR-2 and PAR-6 and a non-essential role of CHIN-1 in the wild-type condition. A reduction in the total concentration of P₂ [PAR-1-PAR-2] reduced the size of the P₂ [PAR-1-PAR-2] domain and shifted the anterior-posterior boundary to the posterior pole (Figure 3F).

In contrast, a decrease in the total concentration of A₁ [CDC-42-PAR-6-PKC-3] enlarged the size of the P₂ [PAR-1-PAR-2] domain and shifted the anterior-posterior boundary to the anterior pole (Figure 3G). Further overexpression of P₂ [PAR-1-PAR-2] induced a bifurcation characterized by high and low cortical concentration of P₂ [PAR-1-PAR-2] and A₂ [PAR-3-PAR-6-PKC-3], respectively, throughout the cortex, while maintaining an anteriorly enriched A₁ [CDC-42-PAR-6-PKC-3] domain (Figure 3H). At the bifurcation point where P₂ [PAR-1-PAR-2] localizes throughout the cortex, a reduction in P₁ [CHIN-1] led to depolarization of the anterior A₁ [CDC-42-PAR-6-PKC-3] domain (Figure 3I), indicating the requirement for CHIN-1 to maintain a

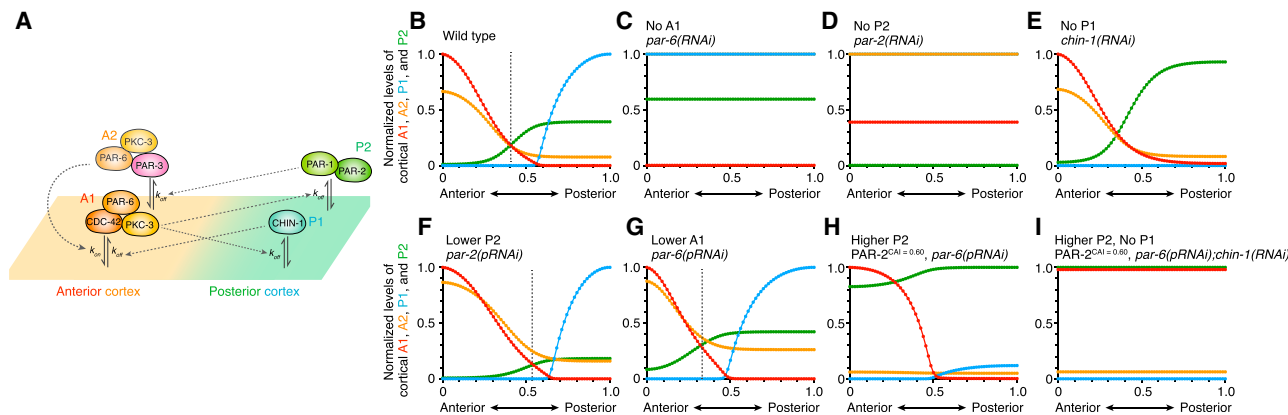


Figure 3. Modeling of a cross-inhibitory PAR network in zygotes

(A) Schematic view of a model of cortical PAR polarity patterning. This model contains four PAR species, including A₁ (CDC-42, PAR-6, and PKC-3), A₂ (PAR-3, PAR-6, and PKC-3), P₁, (CHIN-1), and P₂ (PAR-1 and PAR-2). This scheme includes four inhibitory interactions (from A₁ to P₂, from P₂ to A₂, from A₁ to P₁, and from P₁ to A₁) and one positive interaction (from A₂ to A₁).

(B–I) Steady-state analysis of the model equations in zygotes under following conditions. Predicted distributions of four PAR species at the cortex along the anteroposterior axis are shown. (B) Wild type, (C) no A₁ (par-6(RNAi)), (D) no P₂ (par-2(RNAi)), (E) no P₁ (chin-1(RNAi)), (F) lower P₂ (par-2(pRNAi)), (G) lower A₁ (par-6(pRNAi)), (H) higher P₂ (GFP::PAR-2^{CAI=0.60}, par-6(pRNAi)), and (I) higher P₂ and no P₁ (GFP::PAR-2^{CAI=0.60}, par-6(pRNAi); chin-1(RNAi)).

polarized PAR-6 domain. Thus, our simulation based on the cross-inhibitory network could recapitulate the PAR patterning in zygotes with various balance between PAR proteins.

Reciprocal exclusion of PAR proteins is not essential for the unequal inheritance of fate determinants

We next investigated whether a state characterized by the global pattern of cortical PAR-2 with an anteriorly polarized PAR-6 domain would yield an unequal inheritance of fate determinants during the first cell division. The zygotes with manipulated PAR balances were categorized into three classes based on the distribution patterns of GFP::PAR-2 and fate determinants including PGL-1-positive P-granules and MEX-5, and the position of a cleavage furrow (specified by the position of the mitotic spindle) (see Figure 4 legend for definitions of the phenotypic classes). Both control zygotes and the zygotes with a predominance of PAR-6 (GFP::PAR-2^{CAI=0.26}; mCherry::PAR-6; *Igl-1(dd21)*) segregated PAR proteins, P-granules, MEX-5, and the mitotic spindles (class I zygotes in Figures 4A (i–vi) and 4B–4G). In contrast, more than one-half of the zygotes with a predominance of PAR-2 (GFP::PAR-2^{CAI=0.60}; mCherry::PAR-6, *par-6(pRNAi)* for 9 h) localized GFP::PAR-2 throughout the cortex and exhibited the accumulation of P-granules within the posterior cytoplasm (class II zygotes in Figures 4A (x), 4B, and 4E). These PAR-2-predominant zygotes also established a gradient of MEX-5 enriched within the anterior cytoplasm (class II zygotes in Figures 4A (xi), 4C, and 4F). The mitotic spindles were displaced toward the posterior cortex, resulting in a cleavage furrow positioned toward the posterior pole (class II zygotes in Figures 4A (xii), 4D, and 4G). Both manipulated and control embryos retained cell-cycle asynchrony between AB and P1 cells in two-cell-stage embryos (Figures 5A (ii, iii) and S6A). These observations suggest that these asymmetries between AB and P1 cells were established independently of reciprocal cortical exclusion between PAR-2 and PAR-6 during the first cell division.

The balance between antagonizing PAR proteins specifies the division modes in two-cell-stage embryos

Genetic manipulation of the PAR balances established the PAR-2-predominant zygotes, which achieved the asymmetric inheritance of fate determinants between larger AB cells and smaller P1 cells even with the global pattern of cortical PAR-2 (and an anteriorly polarized PAR-6 domain) during the first cell division. These zygotes enabled us to test whether the abnormal inheritance of PAR proteins would affect the specification of the division modes in AB and P1 cells, while ensuring the correct asymmetries in fate determinants, cell size, and cell-cycle progression between these sister cells. In control embryos expressing normal levels of PAR-2 and PAR-6, the AB cells localized mCherry::PAR-6 and PAR-3 throughout the cortex and GFP::PAR-2 and MEX-5 within the cytoplasm, leading to the equal inheritance of PAR proteins (GFP::PAR-2, mCherry::PAR-6, and PAR-3) and fate determinants (P-granules, MEX-5, and PIE-1) between the two daughter cells (Figures 5A (i, ii), 5B, 5C (i–viii), and 5D). In contrast, PAR-2-predominant AB cells exhibited overlapping distributions of mCherry::PAR-6 and GFP::PAR-2 throughout the cortex during early prophase (Figure 5A (iii)). Subsequently, mCherry::PAR-6 and GFP::PAR-2 began to polarize into two distinct cortical domains, resulting in unequal inheritance of GFP::PAR-2 and mCherry::PAR-6 between the two daughter cells (Figures 5A (iii), 5B, and S6A). The asymmetric segregation of GFP::PAR-2 in AB cells was abolished by severe depletion of PAR-6 (Figure 5A (iv)), suggesting a role of the balance between PAR-2 and PAR-6 in the cortical patterning. The orientation of the two cortical domains occurred randomly with respect to the contact between AB and P1 (Figure S6C), suggesting that the PAR patterning is not instructed by the cell-cell contact. The polarization pattern of GFP::PAR-2 and mCherry::PAR-6 in AB cells was strongly coupled with the polarization of PAR-1 and PAR-3 to their respective cortical domains (Figures 5C (ix–xii) and 5D). Remarkably, the PAR-2-predominant AB cells partitioned cytoplasmic MEX-5 and

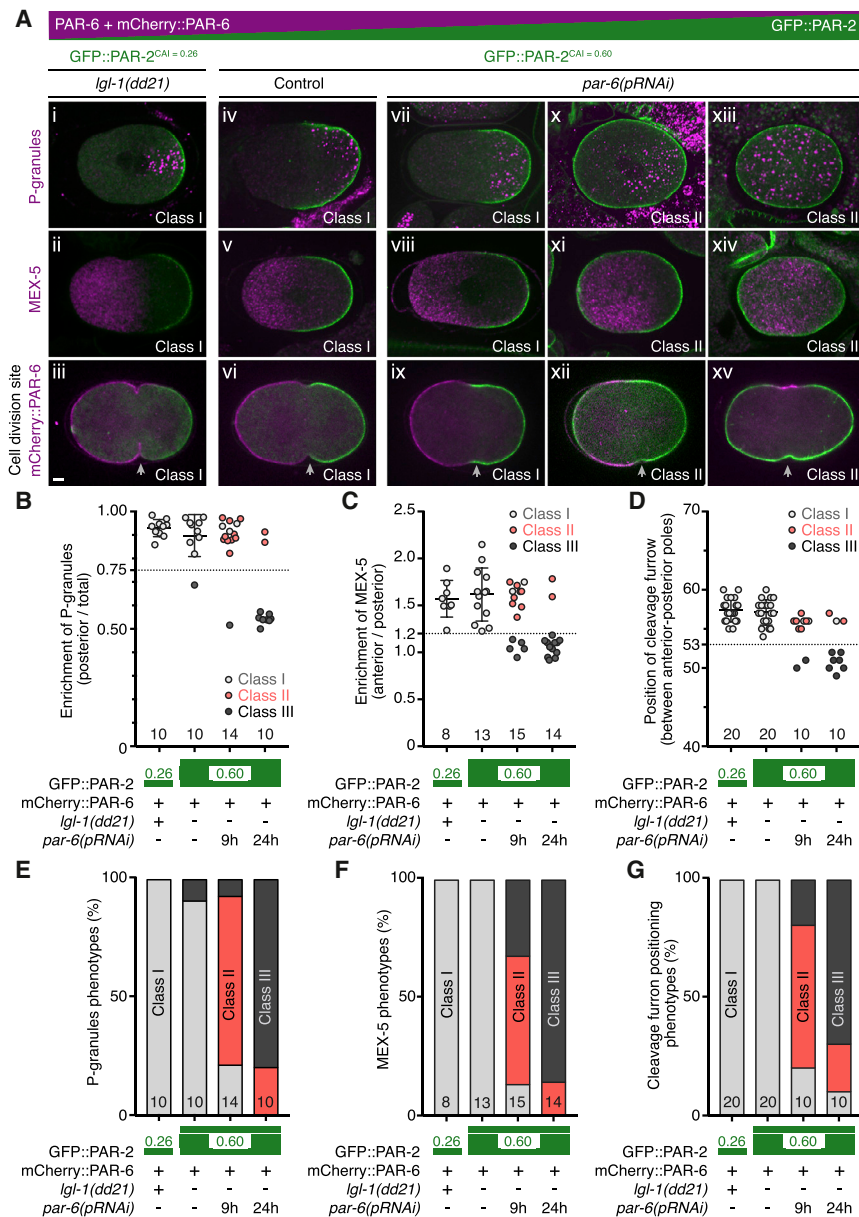


Figure 4. Fate determinants can be segregated independently of reciprocal exclusion between PAR proteins

(A) Representative immunostaining images of GFP::PAR-2 (green) (i–xv) and the cytoplasmic factors such as P-granules (magenta) (i, iv, vii, x, xiii) and MEX-5 (magenta) (ii, v, viii, xi, xiv) and the position of a cleavage furrow (white arrowheads) (iii, vi, ix, xii, xv) in zygotes in which the balance between PAR-6 and PAR-2 was manipulated (using MOT121 strain for GFP::PAR-2^{CAI = 0.26} condition (i–iii) and using MOT120 strain for GFP::PAR-2^{CAI = 0.60} under control (iv–vi) and *par-6(pRNAi)* (vii–xv) conditions). These zygotes were classified into three groups, as follows: class I zygotes established the polarized distributions of GFP::PAR-2 and the cytoplasmic factors (i–ix). Class II zygotes exhibited the polarized distribution of the cytoplasmic factors, whereas GFP::PAR-2 localized throughout the cortex (x–xii). Class III zygotes showed uniform distributions of GFP::PAR-2 and the cytoplasmic factors (xiii–xv). Scale bar, 5 μm. (B–D) The graphs depict the enrichment of P-granules (B) and MEX-5 (C) and the position of cleavage furrows (D) in zygotes described in (A). (E–G) The graphs depict the percentage of three phenotypic classes shown in (B)–(D). (B–G) The number of samples are indicated in the graphs. Height of green bars indicates the CAI values of the *gfp::par-2* transgene.

PIE-1 toward the mCherry::PAR-6 domain and the GFP::PAR-2 domain, respectively (Figures 5C (xiii–xvi), 5D, and S7), indicating the induction of asymmetric division in AB cells. In contrast to AB cells, P1 cells from the same embryos exhibited uniformly distributed GFP::PAR-2 at the cortex and mCherry::PAR-6 in the cytoplasm, resulting in the symmetric division in P1 cells (Figures 5A (iii), 5B, S6, and S7). Based on these observations, we conclude that the manipulation of PAR protein levels is sufficient to reverse the specification of the division modes between AB and P1 cells.

To validate whether changes in the balance of PAR proteins could sufficiently induce asymmetric division in AB cells, we characterized other mutant embryos in which asymmetric inheritance of PAR proteins between AB and P1 cells can be compromised. A previous study demonstrated that mutual exclusion between

the anterior and the posterior PAR domains requires CDC-37 (Beers and Kemphues, 2006). Inhibition of CDC-37 causes symmetric distribution of PAR proteins, with the exception of PAR-3, which exhibits weak enrichment at the anterior cortex (Beers and Kemphues, 2006). Here, *cdc-37(RNAi)* treatment induced the overlapping cortical distributions of mCherry::PAR-6 and GFP::PAR-2 and the symmetric distributions of MEX-5 and P-granules in zygotes (Figures S5A and S5C–S5E). Notably, even in the absence of asymmetric inheritance of PAR-6 during the first cell division, higher levels of GFP::PAR-2^{CAI = 0.60}, but not moderate levels of GFP::PAR-2^{CAI = 0.40}, induced the asymmetric segregation of GFP::PAR-2, PAR-1, PAR-3, MEX-5, and PIE-1 in AB cells of two-cell-stage *cdc-37(RNAi)* embryos (Figures 5A (v, vi), 5B, 5C (xvii–xxiv), 5D, S6A, and S7). These results further suggest that a change in the balance of PAR proteins can sufficiently reverse the division modes between AB and P1 cells.

Next, we investigated whether an optimum level of PAR balance could induce the asymmetric mode of cell division in both sister cells that had equally inherited fate determinants during the first cell division. Here, we aimed to verify whether the specification of the division modes in AB and P1 cells was truly independent of the unequal inheritance of fate determinants and asymmetries in cell size and cell-cycle progression. Using the inhibition of

cyclin-E (CYE-1) to prevent the polarization of PAR proteins due to a failure in the centrosome functions in zygotes (Cowan and Hyman, 2006), we observed the equal inheritance of PAR proteins (mCherry::PAR-6, GFP::PAR-2, and PAR-3) and fate determinants (MEX-5, PIE-1, and P-granules) during the first cell division (Figures S5B, S5C, S5E, and S5F). Moreover, the daughter cells exhibited equal sizes and synchronized cell-cycle progression (Figures 6A (ii, iv) and S6B). In control two-cell-stage embryos, only P1 cells underwent asymmetric inheritance of PAR-2, PAR-3, and fate determinants during mitosis (Figures 6A (i, iii), 6B, 6C (i–viii), and 6D). In two-cell-stage *cye-1(RNAi)* embryos expressing lower levels of GFP::PAR-2^{CAI} = 0.26, both sister cells equally inherited GFP::PAR-2 during mitosis (Figures 6A (iv) and 6B). Remarkably, in two-cell-stage *cye-1(RNAi)* embryos expressing higher levels of GFP::PAR-2^{CAI} = 0.40, both sister cells segregated GFP::PAR-2 to the polar cortex. Consequently, GFP::PAR-2 was inherited unequally by one daughter cell during the two- to four-cell stage (Figures 6A (ii), 6B, and S6B). In these embryos, the polarized distribution of PAR-2 was strongly associated with the segregation of PAR-3 into the respective cortical domain, of MEX-5 in the cytoplasm opposite to the GFP::PAR-2 domain, and of PIE-1 and P-granules toward the GFP::PAR-2 domain (Figures 6C (ix–xvi), 6D, and S7). Based on these observations, we conclude that the selected mode of cell division in two-cell-stage embryos is independent of the unequal inheritance of fate determinants, cell-size asymmetry, and cell-cycle asynchrony between the two sister cells. Our findings support a model that the balance between antagonizing PAR proteins is the intrinsic cue for specification regarding the two cell-division modes in two-cell-stage embryos.

Simulation of PAR patterning in two-cell-stage embryos

To determine whether the specification of the cell-division mode in two-cell-stage embryos can be explained by unequal inheritance of the balance between antagonizing PAR proteins, we applied a mathematical model of the aforementioned PAR network to two-cell-stage embryos (Figures 7A–7E). We performed steady-state analysis of the distribution of PAR species in AB and P1 cells, which are derived from wild-type zygotes or the zygotes with a predominance of PAR-2. Inheritance of the four PAR species between AB and P1 cells was defined by their steady-state distribution in zygotes (Figures 3 and 7A). These PAR species were partitioned at the position of the cleavage furrow measured in the zygotes ($56.1\% \pm 1.6\%$ in wild-type zygotes and $54.8\% \pm 2.3\%$ in PAR-2-predominant zygotes) (Figures 4 and 7A). Wild-type zygotes partitioned the PAR species unequally into two daughter cells. AB cells inherited higher concentrations of A₁ [CDC-42-PAR-6-PKC-3] and A₂ [PAR-3-PAR-6-PKC-3] and lower concentrations of P₁ [CHIN-1] and P₂ [PAR-1-PAR-2] (Figure 7B). The total concentration of the PAR species in P1 cells was determined according to the law of mass conservation (Figure 7B). In wild-type two-cell-stage embryos, all PAR species were symmetrically distributed in AB cells but segregated into two distinct cortical domains in P1 cells (Figure 7C). In PAR-2-predominant zygotes, the inheritance of A₂ [PAR-3-PAR-6-PKC-3] and P₂ [PAR-1-PAR-2] was almost equal, whereas the inheritance of A₁ [CDC-42-PAR-6-PKC-3] and P₁ [CHIN-1] was unequal between the two daughter cells (Figure 7D). In PAR-2-predominant two-cell-stage embryos, A₁ [CDC-42-PAR-6-PKC-3] and A₂ [PAR-3-PAR-6-PKC-3] were

segregated at the anterior cortex and P₁ [CHIN-1] and P₂ [PAR-1-PAR-2] at the posterior cortex in the AB cells, whereas all PAR species were symmetrically distributed in P1 cells (Figure 7E). Our analysis further revealed that the PAR patterning in the PAR-2-predominant embryos was dependent on the unequal inheritance of A₁ [CDC-42-PAR-6-PKC-3], but not in P₁ [CHIN-1], between AB and P1 cells (Figure 8).

We also performed steady-state analysis of the PAR species distribution in two-cell-stage *cye-1(RNAi)* embryos that expressed different levels of PAR-2 (Figures 7F and 7G). In *cye-1(RNAi)* zygotes, all PAR species were equally inherited and divided symmetrically in size, giving rise to two identical daughter cells (Figures S5 and 7F). Because the mechanism triggering symmetry breaking in *cye-1(RNAi)* embryos is unknown, we analyzed a steady-state solution from an initial condition with transient random fluctuations of all PAR species at the cortex. When the level of P₂ [PAR-1-PAR-2] was increased up to 2.5-fold compared to the wild-type condition, A₁ [CDC-42-PAR-6-PKC-3] and A₂ [PAR-3-PAR-6-PKC-3] were segregated to the anterior cortex and P₁ [CHIN-1] and P₂ [PAR-1-PAR-2] to the posterior cortex in both sister cells of *cye-1(RNAi)* embryo (Figure 7G). A reduction in P₂ [PAR-1-PAR-2] of less than 50% caused the symmetric distribution of all PAR species in both sister cells (Figure 7H), indicating that the level of P₂ [PAR-1-PAR-2] is a bifurcation parameter that switches PAR patterning between the polar and apolar states. Therefore, our simulation can recapitulate the PAR patterning in two-cell-stage embryos subjected to manipulation of the balance between PAR proteins. These results suggest that the unequal inheritance of the balance between antagonizing PAR proteins plays a critical role in the specification of PAR patterning in two-cell-stage embryos.

DISCUSSION

In this report, we presented evidence from *C. elegans* embryos indicating that the specification between asymmetric and symmetric modes of cell division relies on the balance between antagonizing PAR proteins. We demonstrated that manipulating the levels of PAR proteins inherited during the first cell division could induce all combinations of asymmetric and/or symmetric patterns of PAR proteins in the daughter cells. The polarized PAR domains artificially induced in these cells were sufficient to establish the unequal inheritance of fate determinants, resulting in successful induction of asymmetric cell division. These results indicate that changes in the balance of PAR proteins are sufficient to re-program the otherwise invariable lineage of the division modes in *C. elegans*. Moreover, the division mode adopted occurred independently of the unequal inheritance of fate determinants, cell-size asymmetry, and cell-cycle asynchrony between the two sister cells. Given that the division modes in two-cell-stage embryos are directed in a cell-autonomous manner (Priess and Thomson, 1987), the intrinsic cue that specifies the division mode must be unequally inherited during the first cell division. We propose that the balance between antagonizing PAR proteins, which should be inherited unequally during the first cell division, is the previously unknown intrinsic

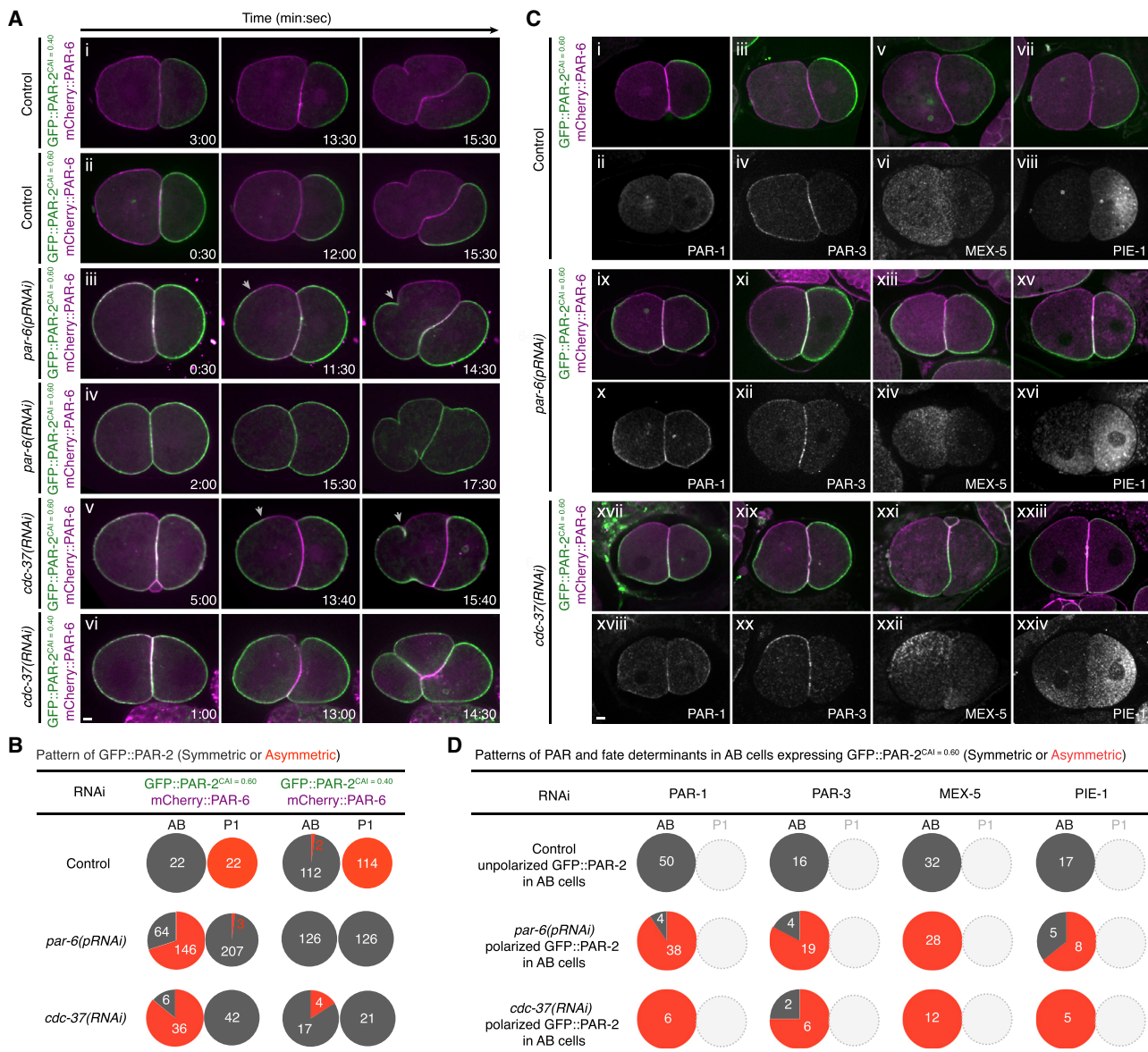


Figure 5. The balance between PAR proteins defines the choice between the two division modes

(A) Changes in the levels of PAR proteins are sufficient to reverse the choice between the two division modes in two-cell-stage embryos. Representative time-lapse images of GFP::PAR-2 (green) and mCherry::PAR-6 (magenta) in live embryos expressing mCherry::PAR-6 and GFP::PAR-2^{CAI = 0.40} (using MOT118 strain) (i, vi) and those expressing mCherry::PAR-6 and GFP::PAR-2^{CAI = 0.60} (using MOT120 strain) (ii–v) under control (i, ii), *par-6(pRNAi)* (iii), *par-6(RNAi)* (iv), and *cdc-37(RNAi)* (v, vi) conditions are shown. Arrowheads show the boundary between mCherry::PAR-6 and GFP::PAR-2 cortical domains. The times stated are with respect to the completion of cytokinesis in zygotes. Scale bar, 5 μm.

(B) The graphs depict the percentage of AB and P1 cells that underwent either equal or unequal inheritance of GFP::PAR-2 under control, *par-6(pRNAi)*, and *cdc-37(RNAi)* conditions.

(C) Induced asymmetry in cortical PAR proteins mediates the segregation of fate determinants in AB cells. Representative immunostaining images of the distributions of PAR-1 (ii, x, xvii), PAR-3 (iv, xii, xx), MEX-5 (vi, xiv, xxii), and PIE-1 (viii, xvi, xxiv) in embryos expressing both mCherry::PAR-6 (magenta) and GFP::PAR-2^{CAI = 0.60} (green) under control (i–viii), *par-6(pRNAi)* (ix–xvi), and *cdc-37(RNAi)* (xvii–xxiv) conditions (using MOT120 strain) are shown. Scale bar, 5 μm.

(D) The graphs depict the percentage of AB cells that segregated PAR-1, PAR-3, MEX-5, and PIE-1 between their daughter cells.

(B and D) The number of cells observed is indicated in the graphs.

cue used to specify the division modes in AB and P1 cells. Our simulation also supports that the balance between antagonizing PAR proteins can be a bifurcation parameter that controls the self-organizing interactions among PAR proteins in

two-cell-stage embryos. A certain balance of PAR protein levels promotes the self-organization of PAR proteins into a mutually exclusive pattern at the cortex, which then mediates the asymmetric mode of cell division. In contrast, a distinct

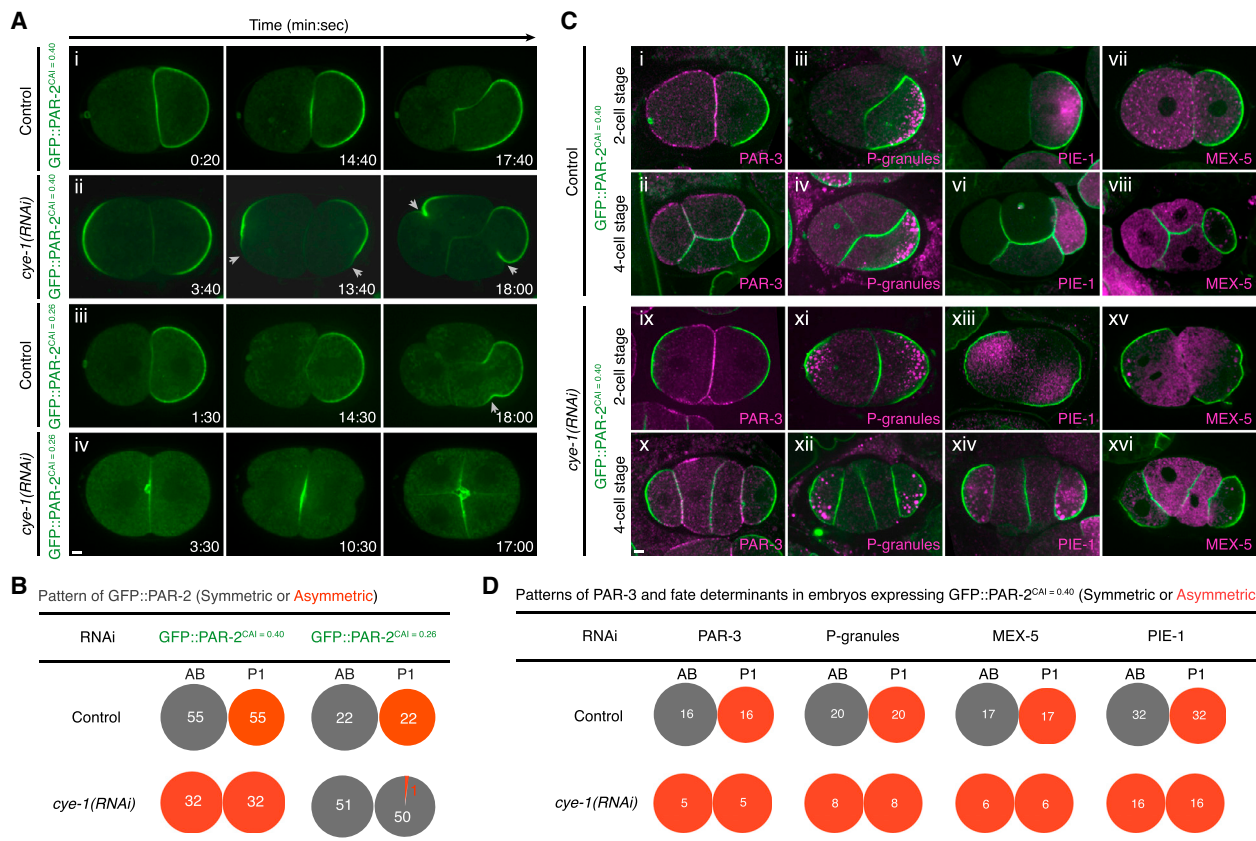


Figure 6. The choice between the two division modes is independent of asymmetries in fate determinants between the sister cells

(A) Unequal inheritance of fate determinants and asymmetries in cell size and cell-cycle progression is not required for determining the two modes of cell division. Representative time-lapse images of GFP::PAR-2 (green) in live embryos expressing GFP::PAR-2^{CAI = 0.40} (using TH413 strain) (i, ii) and those expressing GFP::PAR-2^{CAI = 0.26} (using TH414) (iii, iv) under control (i, iii) and *cye-1(RNAi)* (ii, iv) conditions are shown. Arrowheads show the edges of cortical GFP::PAR-2 domains. The times stated are with respect to the completion of cytokinesis in zygotes. Scale bar, 5 μ m.

(B) The graphs depict the percentage of AB and P1 cells that underwent either equal or unequal inheritance of GFP::PAR-2 between their daughter cells.

(C) Induced asymmetry in cortical PAR proteins in two-cell-stage *cye-1(RNAi)* embryos mediates unequal inheritance of fate determinants. Representative immunostaining images of PAR-3 (i, ii, ix, x), PGL-1-positive P-granules (iii, iv, xi, xii), PIE-1 (v, vi, xiii, xiv), and MEX-5 (vii, viii, xv, xvi) (magenta) in embryos expressing GFP::PAR-2^{CAI = 0.40} (green) under control (i–viii) and *cye-1(RNAi)* (ix–xvi) condition (using TH413 strain) are shown. Scale bar, 5 μ m.

(D) The graphs depict the percentage of the sister cells in two-cell-stage embryos that segregated PAR-3, P-granules, PIE-1, and MEX-5 during the second cell division.

(B and D) The number of cells observed is indicated in the graphs.

balance that does not permit the self-organizing interactions results in the maintenance of unpolarized PAR domains, which then supports the symmetric mode of cell division. During normal development, P1 cells may use a self-organizing mechanism to re-establish the asymmetric distribution of PAR proteins, whereas AB cells exhibit a disproportion in PAR proteins that blocks the self-organization.

PAR proteins have been generally considered downstream effectors of the intrinsic cell-division program. Especially, the segregation of PAR proteins in the *C. elegans* zygotes is controlled by the intrinsic cue from the centrosomes (Klinkert et al., 2019; Reich et al., 2019; Zhao et al., 2019). Recent studies also observed delayed polarization of PAR proteins in zygotes depleted of a centrosome-mediated cue, Aurora-A (Klinkert et al., 2019; Reich et al., 2019; Zhao et al., 2019), suggesting the centrosome-independent self-organization of PAR

proteins. Our findings highlight that the self-organizing property of PAR proteins plays a critical role in the specification of the division modes in two-cell-stage embryos. Although it is not clear as to how the self-organizing interactions among PAR proteins breaks symmetry in two-cell-stage embryos, the process might include amplification of the local spontaneous fluctuations in the concentrations and/or activities of PAR proteins into a global pattern at the cortex. The polarized activities of PAR kinases can, in turn, mediate the cytoplasmic gradient of MEX-5 by increasing its cytoplasmic mobility near the posterior cortical domain (Griffen et al., 2011). The MEX-5 gradient then restricts the activity of the Polo kinase PLK-1 to segregate other fate determinants into the opposite side of the cytoplasm (Han et al., 2018). The MEX-5 gradient also mediates the asymmetric segregation of P-granules by suppressing RNA-mediated liquid-liquid phase transition of PGL proteins and MEG

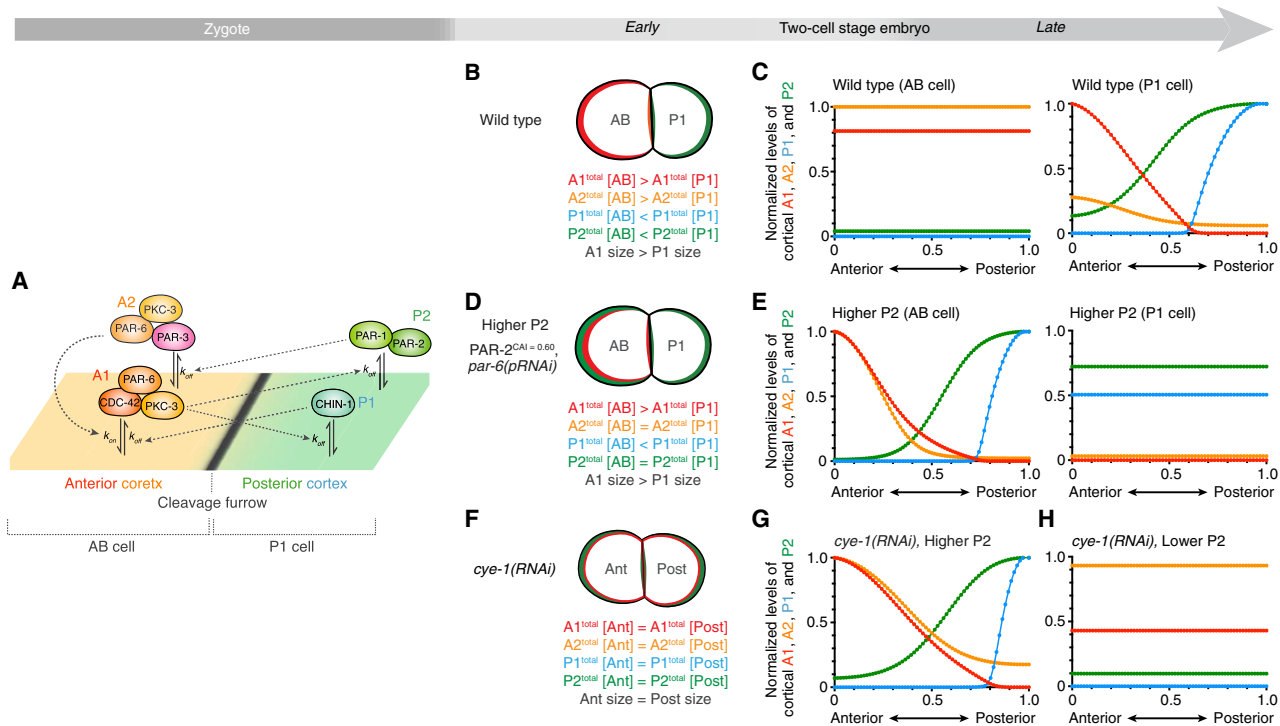


Figure 7. Modeling of a cross-inhibitory PAR network in two-cell-stage embryos

(A) Schematic view of PAR protein inheritance in a wild-type embryo. The four PAR species at steady state in a zygote are partitioned at the position of the cleavage furrow, resulting in unequal inheritance of these PAR species into AB and P1 cells.

(B and C) Steady-state analysis of the PAR network model in a two-cell-stage wild-type embryo. (B) Schematic of PAR-6 (red) and PAR-2 (green) distribution in an AB cell and a P1 cell. (C) Predicted distributions of the PAR species at the cortex along the anteroposterior axis in an AB cell (left) and a P1 cell (right).

(D and E) Steady-state analysis of the PAR network model in a two-cell-stage embryo with a predominance of PAR-2. (D) Schematic of PAR-6 (red) and PAR-2 (green) distribution in an AB cell and a P1 cell. (E) Predicted distributions of the PAR species at the cortex along the anteroposterior axis in an AB cell (left) and a P1 cell (right).

(C and E) Cortical concentration of each PAR species is normalized between AB and P1 cells in the same embryo.

(F–H) Steady-state analysis of the PAR network model in a two-cell-stage *cye-1(RNAi)* embryo. (F) Schematic of PAR-6 (red) and PAR-2 (green) distribution in a *cye-1(RNAi)* embryo. (G and H) Predicted distributions of the PAR species at the cortex along the anteroposterior axis in the daughter cells expressing higher levels of PAR-2 (G) or lower levels of PAR-2 (H). Cortical concentration of each PAR species is normalized between these two conditions.

proteins (Saha et al., 2016; Smith et al., 2016). Based on these findings, we propose that the self-organizing properties of antagonizing PAR proteins serve as active cues that can specify the intrinsic program of the fate-determinant patterning in two-cell-stage embryos.

The comprehensive analysis of zygotes under various balance of PAR proteins has several important implications for understanding the mechanism underlying cortical patterning. Conventionally, the PAR network involves a single reciprocal exclusion pathway among the PAR proteins (Blanchoud et al., 2015; Chau et al., 2012; Dawes and Munro, 2011; Goehring et al., 2011; Gross et al., 2019; Hoege and Hyman, 2013). A recent study proposed an inter-connected cross-inhibitory network between PAR-3-PKC-3-PAR-6-CDC-42 at the anterior cortex and PAR-1-PAR-2 and CHIN-1 at the posterior cortex (Sailer et al., 2015). The results of this study expand these previous models and clarify how multiple PAR complexes can be inter-connected and orchestrated to pattern cortical domains. In the revised model, a cross-inhibitory network of PAR proteins containing PAR-3-PAR-6-PKC-

3, CDC-42-PAR-6-PKC-3, and PAR-1-PAR-2 is complemented by another cross-inhibitory network involving CDC-42-PAR-6-PKC-3 and CHIN-1. Our current model for the polarized activity of CDC-42 considers its global activation by the guanine nucleotide exchange factor CGEF-1 (Kumfer et al., 2010) and its local inactivation by CHIN-1 at the posterior cortex, although CGEF-1 activity may be spatially biased toward the anterior cortex. Our simulations based on a revised cross-inhibitory network recapitulate the cortical patterning of PAR proteins in zygotes under various balances of PAR proteins. Indeed, the robustness of the cross-inhibitory network enables uncoupling of the inheritance of PAR proteins from that of fate determinants during the first cell division. Our findings are consistent with previous observations wherein several alleles of *par* mutants failed to establish the reciprocal exclusion of PAR proteins but induced the polarization of P-granules (Bowerman et al., 1997; Boyd et al., 1996; Kemphues et al., 1988; Morton et al., 2002). Our observations also reveal that the reciprocal exclusion of PAR proteins is not necessary for the unequal inheritance of fate determinants in zygotes.

Although both PAR-1 and PAR-2 exhibited uniform cortical distribution in PAR-2-predominant zygotes, the activity of the posterior PAR complex may be spatially segregated. Indeed, a recent study by [Folkmann and Seydoux \(2019\)](#) suggested the modular regulation of the PAR-1 activity by autoinhibition by the KA1 domain and phosphorylation by PKC-3. Such dual regulation of the PAR-1 activity could contribute to the segregation of fate determinants in the PAR-2-predominant zygotes.

Previous studies have implicated PAR polarity in cortical polarization and asymmetric cell division in many cell types, including *Drosophila* neuroblasts ([Knoblich, 2010](#)), vertebrate embryos ([Maître et al., 2016](#)), neural progenitor cells ([Homem et al., 2015](#)), and several types of stem cells ([Chang et al., 2007](#); [Dumont et al., 2015](#); [Lechler and Fuchs, 2005](#)). The striking conservation of the function of PAR proteins in both invertebrates and vertebrates raises a possibility that the self-organizing PAR system is a conserved executor of the specification between the two division modes. Consistent with this model, a recent study also revealed that overexpression of *Drosophila* PAR-3, Bazooka, is sufficient to trigger the segregation of other PAR proteins and fate determinants in S2 cells ([Kono et al., 2019](#)). Interestingly, the ratios of PAR proteins can be modified dynamically during development. For example, the ratio of PAR-3 to PAR-1 is actively modified to induce morphogenetic movement in the *Drosophila* epithelium ([Wang et al., 2012](#)). It is therefore tempting to speculate that the balance between antagonizing PAR proteins could be controlled dynamically to affect the facultative choice between the two modes of cell division during development. Indeed, many types of stem cells shift between these modes to balance the needs of self-renewal and cell differentiation ([Morrison and Kimble, 2006](#)). Hence, our findings suggest that the dynamic control of cortical polarization is directly linked to the specification regarding the asymmetric or symmetric mode of cell division, a critical decision faced by every single cell in a multicellular organism.

STAR★METHODS

Detailed methods are provided in the online version of this paper and include the following:

- [KEY RESOURCES TABLE](#)
- [RESOURCE AVAILABILITY](#)
 - Lead contact
 - Materials availability
 - Data and code availability
- [EXPERIMENTAL MODEL AND SUBJECT DETAILS](#)
- [METHOD DETAILS](#)
 - RNA interference (RNAi)
 - Imaging of *C. elegans* embryos
 - Modeling of PAR polarity in zygotes
 - Modeling of PAR polarity in two-cell-stage embryos
- [QUANTIFICATION AND STATISTICAL ANALYSIS](#)
 - Quantification of PAR proteins and fate determinants
 - Statistical tests and reproducibility

SUPPLEMENTAL INFORMATION

Supplemental information can be found online at <https://doi.org/10.1016/j.celrep.2021.109326>.

ACKNOWLEDGMENTS

This study was supported by the Singapore National Research Foundation (NRF-NRFF2012-08 [F.M.]) and the Strategic Japan-Singapore Cooperative Research Program by the Japan Science and Technology Agency and the Singapore Agency for Science, Technology, and Research (1514324022 [F.M.] and 15658064 [T.S.]), the core funding at RIKEN Center for Biosystems Dyamics Research (T.S.), and RIKEN Special Post-doctoral Researcher Program (F.-L.W.). We are grateful to Nathan Goehring (The Francis Crick Institute), Pierre Gonczi (EPFL), Monica Gotta (University of Geneva), Carsten Hoege and Anthony Hyman (MPI), Ken Kemphues (Cornell University), Jean-Claude Labbe (IRIC), Shibi Mathew (Temasek Life-sciences Laboratory), Geraldine Seydoux (Johns Hopkins University), Shigeo Ohno (Yokohama-City University), Zhen Zhang and Pakorn Kanchanawong (Mechanobiology Institute, Singapore), and the Caenorhabditis Genetic Center for strains, reagents, and expertise. We also thank Andrew Wong (Mechanobiology Institute, Singapore) and members in the Motegi lab for comments on the manuscript.

AUTHOR CONTRIBUTIONS

The experimental design and presented ideas were developed together by all authors. F.M. guided the study and wrote the manuscript with input from all authors. Y.W.L. performed all experiments. F.-L.W., P.S., and T.S. developed the theoretical models for an inter-connecting network of two reciprocal cortical exclusion pathways.

DECLARATION OF INTERESTS

The authors declare no competing financial interests.

Received: August 18, 2020

Revised: March 5, 2021

Accepted: June 8, 2021

Published: July 6, 2021

REFERENCES

- Aceto, D., Beers, M., and Kemphues, K.J. (2006). Interaction of PAR-6 with CDC-42 is required for maintenance but not establishment of PAR asymmetry in *C. elegans*. *Dev. Biol.* **299**, 386–397.
- Beatty, A., Morton, D., and Kemphues, K. (2010). The *C. elegans* homolog of *Drosophila* Lethal giant larvae functions redundantly with PAR-2 to maintain polarity in the early embryo. *Development* **137**, 3995–4004.
- Beers, M., and Kemphues, K. (2006). Depletion of the co-chaperone CDC-37 reveals two modes of PAR-6 cortical association in *C. elegans* embryos. *Development* **133**, 3745–3754.
- Blanchoud, S., Busso, C., Naef, F., and Gönczy, P. (2015). Quantitative analysis and modeling probe polarity establishment in *C. elegans* embryos. *Bioophys. J.* **108**, 799–809.
- Bowerman, B., Ingram, M.K., and Hunter, C.P. (1997). The maternal par genes and the segregation of cell fate specification activities in early *Caenorhabditis elegans* embryos. *Development* **124**, 3815–3826.
- Boyd, L., Guo, S., Levitan, D., Stinchcomb, D.T., and Kemphues, K.J. (1996). PAR-2 is asymmetrically distributed and promotes association of P granules and PAR-1 with the cortex in *C. elegans* embryos. *Development* **122**, 3075–3084.
- Chang, J.T., Palanivel, V.R., Kinjyo, I., Schambach, F., Intlekofer, A.M., Banerjee, A., Longworth, S.A., Vinup, K.E., Mrass, P., Oliaro, J., et al. (2007). Asymmetric T lymphocyte division in the initiation of adaptive immune responses. *Science* **315**, 1687–1691.

- Chau, A.H., Walter, J.M., Gerardin, J., Tang, C., and Lim, W.A. (2012). Designing synthetic regulatory networks capable of self-organizing cell polarization. *Cell* 151, 320–332.
- Chen, C., Fingerhut, J.M., and Yamashita, Y.M. (2016). The ins(ide) and outs(ide) of asymmetric stem cell division. *Curr. Opin. Cell Biol.* 43, 1–6.
- Cheng, N.N., Kirby, C.M., and Kemphues, K.J. (1995). Control of cleavage spindle orientation in *Caenorhabditis elegans*: the role of the genes par-2 and par-3. *Genetics* 139, 549–559.
- Cowan, C.R., and Hyman, A.A. (2006). Cyclin E-Cdk2 temporally regulates centrosome assembly and establishment of polarity in *Caenorhabditis elegans* embryos. *Nat. Cell Biol.* 8, 1441–1447.
- Cuenca, A.A., Schetter, A., Aceto, D., Kemphues, K., and Seydoux, G. (2003). Polarization of the *C. elegans* zygote proceeds via distinct establishment and maintenance phases. *Development* 130, 1255–1265.
- Dawes, A.T., and Munro, E.M. (2011). PAR-3 oligomerization may provide an actin-independent mechanism to maintain distinct par protein domains in the early *Caenorhabditis elegans* embryo. *Biophys. J.* 101, 1412–1422.
- Dumont, N.A., Bentzinger, C.F., Sincennes, M.C., and Rudnicki, M.A. (2015). Satellite Cells and Skeletal Muscle Regeneration. *Compr. Physiol.* 5, 1027–1059.
- Etemad-Moghadam, B., Guo, S., and Kemphues, K.J. (1995). Asymmetrically distributed PAR-3 protein contributes to cell polarity and spindle alignment in early *C. elegans* embryos. *Cell* 83, 743–752.
- Folkmann, A.W., and Seydoux, G. (2019). Spatial regulation of the polarity kinase PAR-1 by parallel inhibitory mechanisms. *Development* 146, dev171116.
- Goehring, N.W., Trong, P.K., Bois, J.S., Chowdhury, D., Nicola, E.M., Hyman, A.A., and Grill, S.W. (2011). Polarization of PAR proteins by advective triggering of a pattern-forming system. *Science* 334, 1137–1141.
- Goldstein, B., and Macara, I.G. (2007). The PAR proteins: fundamental players in animal cell polarization. *Dev. Cell* 13, 609–622.
- Gönczy, P., Bellanger, J.M., Kirkham, M., Pozniakowski, A., Baumer, K., Phillips, J.B., and Hyman, A.A. (2001). zyg-8, a gene required for spindle positioning in *C. elegans*, encodes a doublecortin-related kinase that promotes microtubule assembly. *Dev. Cell* 1, 363–375.
- Gotta, M., and Ahringer, J. (2001). Distinct roles for Galpha and Gbetagamma in regulating spindle position and orientation in *Caenorhabditis elegans* embryos. *Nat. Cell Biol.* 3, 297–300.
- Gotta, M., Dong, Y., Peterson, Y.K., Lanier, S.M., and Ahringer, J. (2003). Asymmetrically distributed *C. elegans* homologs of AGS3/PINS control spindle position in the early embryo. *Curr. Biol.* 13, 1029–1037.
- Griffen, E.E., Odde, D.J., and Seydoux, G. (2011). Regulation of the MEX-5 gradient by a spatially segregated kinase/phosphatase cycle. *Cell* 146, 955–968.
- Griffin, E.E. (2015). Cytoplasmic localization and asymmetric division in the early embryo of *Caenorhabditis elegans*. *Wiley Interdiscip. Rev. Dev. Biol.* 4, 267–282.
- Griffin, E.E., Odde, D.J., and Seydoux, G. (2011). Regulation of the MEX-5 gradient by a spatially segregated kinase/phosphatase cycle. *Cell* 146, 955–968.
- Gross, P., Kumar, K.V., Goehring, N.W., Bois, J.S., Hoege, C., Jülicher, F., and Grill, S.W. (2019). Guiding self-organized pattern formation in cell polarity establishment. *Nat. Phys.* 15, 293–300.
- Guo, S., and Kemphues, K.J. (1995). par-1, a gene required for establishing polarity in *C. elegans* embryos, encodes a putative Ser/Thr kinase that is asymmetrically distributed. *Cell* 81, 611–620.
- Han, B., Antkowiak, K.R., Fan, X., Rutigliano, M., Ryder, S.P., and Griffin, E.E. (2018). Polo-like kinase couples cytoplasmic protein gradients in the *C. elegans* zygote. *Curr. Biol.* 28, 60–69.e8.
- Hoege, C., and Hyman, A.A. (2013). Principles of PAR polarity in *Caenorhabditis elegans* embryos. *Nat. Rev. Mol. Cell Biol.* 14, 315–322.
- Hoege, C., Constantinescu, A.T., Schwager, A., Goehring, N.W., Kumar, P., and Hyman, A.A. (2010). LGL can partition the cortex of one-cell *Caenorhabditis elegans* embryos into two domains. *Curr. Biol.* 20, 1296–1303.
- Homem, C.C., Repic, M., and Knoblich, J.A. (2015). Proliferation control in neural stem and progenitor cells. *Nat. Rev. Neurosci.* 16, 647–659.
- Horvitz, H.R., and Herskowitz, I. (1992). Mechanisms of asymmetric cell division: two Bs or not two Bs, that is the question. *Cell* 68, 237–255.
- Hung, T.J., and Kemphues, K.J. (1999). PAR-6 is a conserved PDZ domain-containing protein that colocalizes with PAR-3 in *Caenorhabditis elegans* embryos. *Development* 126, 127–135.
- Joberty, G., Petersen, C., Gao, L., and Macara, I.G. (2000). The cell-polarity protein Par6 links Par3 and atypical protein kinase C to Cdc42. *Nat. Cell Biol.* 2, 531–539.
- Kemphues, K. (2000). PARsing embryonic polarity. *Cell* 101, 345–348.
- Kemphues, K.J., Priess, J.R., Morton, D.G., and Cheng, N.S. (1988). Identification of genes required for cytoplasmic localization in early *C. elegans* embryos. *Cell* 52, 311–320.
- Klinkert, K., Levernier, N., Gross, P., Gentili, C., von Tobel, L., Pierron, M., Busso, C., Herrman, S., Grill, S.W., Kruse, K., and Gönczy, P. (2019). Aurora A depletion reveals centrosome-independent polarization mechanism in *Caenorhabditis elegans*. *eLife* 8, e44552.
- Knoblich, J.A. (2008). Mechanisms of asymmetric stem cell division. *Cell* 132, 583–597.
- Knoblich, J.A. (2010). Asymmetric cell division: recent developments and their implications for tumour biology. *Nat. Rev. Mol. Cell Biol.* 11, 849–860.
- Kono, K., Yoshiura, S., Fujita, I., Okada, Y., Shitamukai, A., Shibata, T., and Matsuzaki, F. (2019). Reconstruction of Par-dependent polarity in apolar cells reveals a dynamic process of cortical polarization. *eLife* 8, e45559.
- Kotak, S. (2019). Mechanisms of Spindle Positioning: Lessons from Worms and Mammalian Cells. *Biomolecules* 9, 80.
- Kumfer, K.T., Cook, S.J., Squirrell, J.M., Eliceiri, K.W., Peel, N., O'Connell, K.F., and White, J.G. (2010). CGEF-1 and CHIN-1 regulate CDC-42 activity during asymmetric division in the *Caenorhabditis elegans* embryo. *Mol. Biol. Cell* 21, 266–277.
- Lechler, T., and Fuchs, E. (2005). Asymmetric cell divisions promote stratification and differentiation of mammalian skin. *Nature* 437, 275–280.
- Maître, J.L., Turlier, H., Illukkumbura, R., Eismann, B., Niwayama, R., Nédélec, F., and Hiiragi, T. (2016). Asymmetric division of contractile domains couples cell positioning and fate specification. *Nature* 536, 344–348.
- Morrison, S.J., and Kimble, J. (2006). Asymmetric and symmetric stem-cell divisions in development and cancer. *Nature* 441, 1068–1074.
- Morton, D.G., Shakes, D.C., Nugent, S., Dichoso, D., Wang, W., Golden, A., and Kemphues, K.J. (2002). The *Caenorhabditis elegans* par-5 gene encodes a 14-3-3 protein required for cellular asymmetry in the early embryo. *Dev. Biol.* 241, 47–58.
- Motegi, F., Zonies, S., Hao, Y., Cuenca, A.A., Griffin, E., and Seydoux, G. (2011). Microtubules induce self-organization of polarized PAR domains in *Caenorhabditis elegans* zygotes. *Nat. Cell Biol.* 13, 1361–1367.
- Pacquelet, A., Zanin, E., Ashiono, C., and Gotta, M. (2008). PAR-6 levels are regulated by NOS-3 in a CUL-2 dependent manner in *Caenorhabditis elegans*. *Dev. Biol.* 319, 267–272.
- Priess, J.R., and Thomson, J.N. (1987). Cellular interactions in early *C. elegans* embryos. *Cell* 48, 241–250.
- Redemann, S., Weber, B., Möller, M., Verbavatz, J.M., Hyman, A.A., Baum, D., Prohaska, S., and Müller-Reichert, T. (2014). The segmentation of microtubules in electron tomograms using Amira. *Methods Mol. Biol.* 1136, 261–278.
- Reich, J.D., Hubatsch, L., Illukkumbura, R., Peglion, F., Bland, T., Hirani, N., and Goehring, N.W. (2019). Regulated Activation of the PAR Polarity Network Ensures a Timely and Specific Response to Spatial Cues. *Curr. Biol.* 29, 1911–1923.e1915.
- Rodriguez, J., Peglion, F., Martin, J., Hubatsch, L., Reich, J., Hirani, N., Guibieda, A.G., Roffey, J., Fernandes, A.R., St Johnston, D., et al. (2017). aPKC

- Cycles between Functionally Distinct PAR Protein Assemblies to Drive Cell Polarity. *Dev. Cell* 42, 400–415.e9.
- Rose, L., and Gonczy, P. (2014). Polarity establishment, asymmetric division and segregation of fate determinants in early *C. elegans* embryos. *WormBook*, 1–43.
- Saha, S., Weber, C.A., Nousch, M., Adame-Arana, O., Hoege, C., Hein, M.Y., Osbourne-Nishimura, E., Mahamid, J., Jahnel, M., Jawerth, L., et al. (2016). Polar Positioning of Phase-Separated Liquid Compartments in Cells Regulated by an mRNA Competition Mechanism. *Cell* 166, 1572–1584.e16.
- Sailer, A., Anneken, A., Li, Y., Lee, S., and Munro, E. (2015). Dynamic Opposition of Clustered Proteins Stabilizes Cortical Polarity in the *C. elegans* Zygote. *Dev. Cell* 35, 131–142.
- Schubert, C.M., Lin, R., de Vries, C.J., Plasterk, R.H., and Priess, J.R. (2000). MEX-5 and MEX-6 function to establish soma/germline asymmetry in early *C. elegans* embryos. *Mol. Cell* 5, 671–682.
- Seydoux, G., and Dunn, M.A. (1997). Transcriptionally repressed germ cells lack a subpopulation of phosphorylated RNA polymerase II in early embryos of *Caenorhabditis elegans* and *Drosophila melanogaster*. *Development* 124, 2191–2201.
- Seydoux, G., Mello, C.C., Pettitt, J., Wood, W.B., Priess, J.R., and Fire, A. (1996). Repression of gene expression in the embryonic germ lineage of *C. elegans*. *Nature* 382, 713–716.
- Singh, D., and Pohl, C. (2014). Coupling of rotational cortical flow, asymmetric midbody positioning, and spindle rotation mediates dorsoventral axis formation in *C. elegans*. *Dev. Cell* 28, 253–267.
- Smith, J., Calidas, D., Schmidt, H., Lu, T., Rasoloson, D., and Seydoux, G. (2016). Spatial patterning of P granules by RNA-induced phase separation of the intrinsically-disordered protein MEG-3. *eLife* 5, e21337.
- Sugioka, K., and Bowerman, B. (2018). Combinatorial Contact Cues Specify Cell Division Orientation by Directing Cortical Myosin Flows. *Dev. Cell* 46, 257–270.e5.
- Sulston, J.E., and Horvitz, H.R. (1977). Post-embryonic cell lineages of the nematode, *Caenorhabditis elegans*. *Dev. Biol.* 56, 110–156.
- Sulston, J.E., Schierenberg, E., White, J.G., and Thomson, J.N. (1983). The embryonic cell lineage of the nematode *Caenorhabditis elegans*. *Dev. Biol.* 100, 64–119.
- Tabuse, Y., Izumi, Y., Piano, F., Kemphues, K.J., Miwa, J., and Ohno, S. (1998). Atypical protein kinase C cooperates with PAR-3 to establish embryonic polarity in *Caenorhabditis elegans*. *Development* 125, 3607–3614.
- Wang, Y.C., Khan, Z., Kaschube, M., and Wieschaus, E.F. (2012). Differential positioning of adherens junctions is associated with initiation of epithelial folding. *Nature* 484, 390–393.
- Wang, S.C., Low, T.Y.F., Nishimura, Y., Gole, L., Yu, W., and Motegi, F. (2017). Cortical forces and CDC-42 control clustering of PAR proteins for *Caenorhabditis elegans* embryonic polarization. *Nat. Cell Biol.* 19, 988–995.
- Zhang, Z., Lim, Y.W., Zhao, P., Kanchanawong, P., and Motegi, F. (2017). Im-aEdge: a platform for the quantitative analysis of cortical proteins spatiotemporal dynamics during cell polarization. *J. Cell Sci.* 130, 4200–4212.
- Zhao, P., Teng, X., Tantirimudalige, S.N., Nishikawa, M., Wohland, T., Toyama, Y., and Motegi, F. (2019). Aurora-A Breaks Symmetry in Contractile Actomyosin Networks Independently of Its Role in Centrosome Maturation. *Dev. Cell* 48, 631–645.e6.

STAR★METHODS

KEY RESOURCES TABLE

REAGENT or RESOURCE	SOURCE	IDENTIFIER
Antibodies		
Rabbit polyclonal anti-PAR-1	Hoege et al., 2010	N/A
Rabbit polyclonal anti-PAR-1	Gönczy et al., 2001	N/A
Rabbit polyclonal anti-PAR-2	Hoege et al., 2010	N/A
Mouse monoclonal anti-PAR-3	DSHB	P4A1
Rabbit polyclonal anti-PAR-6	This study	N/A
Mouse monoclonal anti-PGL-1	DSHB	OIC1D4
Mouse monoclonal anti-MEX-5	Schubert et al., 2000	N/A
Donkey anti-rabbit IgG coupled to Cy5	Jackson ImmunoResearch	711-175-152
Donkey anti-mouse IgG coupled to Cy5	Jackson ImmunoResearch	711-175-150
Goat anti-rabbit IgG coupled to Cy3	Abcam	Ab6939
Goat anti-mouse IgG coupled to Cy3	Abcam	Ab97035
Goat anti-rabbit IgG coupled to Alexa Fluor 594	Lab-Chem Enzyme	A11005
Goat anti-mouse IgG coupled to Alexa Fluor 594	Lab-Chem Enzyme	A11012
Bacterial and virus strains		
<i>E. coli</i> : HT115(DE3): F-, mcrA, mcrB, IN(rrnD-rrnE)1, rnc14::Tn10(DE3) lysogen: lacUV5 promoter -T7 polymerase) (IPTG-inducible T7 polymerase) (RNase III minus).	Caenorhabditis Genetics Center	HT115(DE3)
<i>E. coli</i> : OP50: <i>E. coli</i> B, uracil auxotroph	Caenorhabditis Genetics Center	OP50
Chemicals, peptides, and recombinant proteins		
Vectashield Mounting Medium with DAPI	Vector Laboratories	Cat# H-1200
Poly-Lysine L-lysine hydrobromide	Sigma-Aldrich	Cat# P1524
IPTG	Gold Biotechnology	Cat# I2481C100
20 µm monodisperse polystyrene beads	Bangs Laboratories	Cat# PS07003
Megascript T7 Transcription kit	Invitrogen	AMB13345
Experimental models: Organisms/strains		
<i>C. elegans</i> : Strain N2: Wild type	Caenorhabditis Genetics Center	N2
<i>C. elegans</i> : Strain JH2952: unc-119(ed3) III; tems7[pIC26::par-2 re-coded], par-2(ok1723)	Motegi et al., 2011	JH2952
<i>C. elegans</i> : Strain TH413: unc-119(ed3) III; ddls25[gfp::par-2 re-coded, CAI = 0.41]; par-2(ok1723)	Goehring et al., 2011	TH413
<i>C. elegans</i> : Strain TH414: unc-119(ed3) III; ddls238[gfp::par-2 re-coded, CAI = 0.26]; par-2(ok1723)	Goehring et al., 2011	TH414
<i>C. elegans</i> : Strain TH415: unc-119(ed3) III; ddls239[gfp::par-2 re-coded, CAI = 0.60]; par-2(ok1723)	Goehring et al., 2011	TH415

(Continued on next page)

Continued

REAGENT or RESOURCE	SOURCE	IDENTIFIER
<i>C. elegans</i> : Strain MOT119: <i>unc-119(ed3)</i> <i>III</i> ; <i>ddls238[gfp::par-2 re-coded, CAI = 0.26]; par-2(ok1723); temls17[piet-1p::mcherry::par-6::pie-1 3'UTR]</i>	Zhang et al., 2017	MOT119
<i>C. elegans</i> : Strain MOT121: <i>unc-119(ed3)</i> <i>III</i> ; <i>temls7[pIC26::par-2 re-coded], par-2(ok1723); temls17[piet-1p::mcherry::par-6::pie-1 3'UTR]</i>	Zhang et al., 2017	MOT121
<i>C. elegans</i> : Strain MOT118: <i>unc-119(ed3)</i> <i>III; ddls25[gfp::par-2 re-coded, CAI = 0.41]; par-2(ok1723); temls17[piet-1p::mcherry::par-6::pie-1 3'UTR]</i>	Zhang et al., 2017	MOT118
<i>C. elegans</i> : Strain MOT120: <i>unc-119(ed3)</i> <i>III; ddls239[gfp::par-2 re-coded, CAI = 0.60]; par-2(ok1723); temls17[piet-1p::mcherry::par-6::pie-1 3'UTR]</i>	Zhang et al., 2017	MOT120
<i>C. elegans</i> : Strain MOT401: <i>unc-119(ed3)</i> <i>III; ddls239[gfp::par-2 re-coded, CAI = 0.60]; par-2(ok1723); temls17[piet-1p::mcherry::par-6::pie-1 3'UTR]; axls1464[piet-1p::gfp::pgl-3::piet-1 3'UTR]</i>	This study	MOT401
<i>C. elegans</i> : Strain MOT175: <i>unc-119(ed3)</i> <i>III; temls7[pIC26::par-2 re-coded], par-2(ok1723); nos-3(q650) II</i>	This study	MOT175
<i>C. elegans</i> : Strain MOT177: <i>unc-119(ed3)</i> <i>III; ddls25[gfp::par-2 re-coded, CAI = 0.41]; par-2(ok1723); nos-3(q650) II</i>	This study	MOT177
<i>C. elegans</i> : Strain MOT179: <i>unc-119(ed3)</i> <i>III; ddls238[gfp::par-2 re-coded, CAI = 0.26]; par-2(ok1723); nos-3(q650) II</i>	This study	MOT179
<i>C. elegans</i> : Strain MOT183: <i>unc-119(ed3)</i> <i>III; ddls239[gfp::par-2 re-coded, CAI = 0.60]; par-2(ok1723); nos-3(q650) II</i>	This study	MOT183
<i>C. elegans</i> : Strain MOT176: <i>unc-119(ed3)</i> <i>III; ddls238[gfp::par-2 re-coded, CAI = 0.26]; par-2(ok1723); temls17[piet-1p::mcherry::par-6::pie-1 3'UTR]; nos-3(q650) II</i>	This study	MOT176
<i>C. elegans</i> : Strain MOT178: <i>unc-119(ed3)</i> <i>III; temls7[pIC26::par-2 re-coded], par-2(ok1723); temls17[piet-1p::mcherry::par-6::pie-1 3'UTR]; nos-3(q650) II</i>	This study	MOT178
<i>C. elegans</i> : Strain MOT180: <i>unc-119(ed3)</i> <i>III; ddls25[gfp::par-2 re-coded, CAI = 0.41]; par-2(ok1723); temls17[piet-1p::mcherry::par-6::pie-1 3'UTR]; nos-3(q650) II</i>	This study	MOT180
<i>C. elegans</i> : Strain MOT184: <i>unc-119(ed3)</i> <i>III; ddls239[gfp::par-2 re-coded, CAI = 0.60]; par-2(ok1723); temls17[piet-1p::mcherry::par-6::pie-1 3'UTR]; nos-3(q650) II</i>	This study	MOT184
<i>C. elegans</i> : Strain MOT192: <i>unc-119(ed3)</i> <i>III; temls7[pIC26::par-2 re-coded], par-2(ok1723); lgl-1(dd21) X</i>	This study	MOT192

(Continued on next page)

Continued

REAGENT or RESOURCE	SOURCE	IDENTIFIER
<i>C. elegans</i> : Strain MOT190: <i>unc-119(ed3) III; ddls25[gfp::par-2 re-coded, CAI = 0.41]; par-2(ok1723); lgl-1(dd21) X</i>	This study	MOT190
<i>C. elegans</i> : Strain MOT185: <i>unc-119(ed3) III; ddls238[gfp::par-2 re-coded, CAI = 0.26]; par-2(ok1723); lgl-1(dd21) X</i>	This study	MOT185
<i>C. elegans</i> : Strain MOT199: <i>unc-119(ed3) III; ddls239[gfp::par-2 re-coded, CAI = 0.60]; par-2(ok1723); lgl-1(dd21) X</i>	This study	MOT199
<i>C. elegans</i> : Strain MOT186: <i>unc-119(ed3) III; ddls238[gfp::par-2 re-coded, CAI = 0.26]; par-2(ok1723); temls17[pi-e-1p::mcherry::par-6::pi-e-1 3'UTR]; lgl-1(dd21) X</i>	This study	MOT186
<i>C. elegans</i> : Strain MOT188: <i>unc-119(ed3) III; temls7[plC26::par-2 re-coded]; par-2(ok1723); temls17[pi-e-1p::mcherry::par-6::pi-e-1 3'UTR]; lgl-1(dd21) X</i>	This study	MOT188
<i>C. elegans</i> : Strain MOT189: <i>unc-119(ed3) III; ddls25[gfp::par-2 re-coded, CAI = 0.41]; par-2(ok1723); temls17[pi-e-1p::mcherry::par-6::pi-e-1 3'UTR]; lgl-1(dd21) X</i>	This study	MOT189
<i>C. elegans</i> : Strain MOT191: <i>unc-119(ed3) III; ddls239[gfp::par-2 re-coded, CAI = 0.60]; par-2(ok1723); temls17[pi-e-1p::mcherry::par-6::pi-e-1 3'UTR]; lgl-1(dd21) X</i>	This study	MOT191
<i>C. elegans</i> : Strain JK2589: <i>nos-3(q650) II</i>	Pacquelet et al., 2008	JK2589
<i>C. elegans</i> : Strain TH131: <i>lgl-1(dd21) X</i>	Hoege et al., 2010	TH131
<i>C. elegans</i> : Strain MOT660: <i>par-6(cp60[par-6::mKate2::3xMyc + LoxP unc-119(+)] I; unc-119(ed3) III; ddls25[gfp::par-2 re-coded, CAI = 0.41]; par-2(ok1723)</i>	This study	MOT660
<i>C. elegans</i> : Strain MOT661: <i>par-6(cp60[par-6::mKate2::3xMyc + LoxP unc-119(+)] I; unc-119(ed3) III; ddls238[gfp::par-2 re-coded, CAI = 0.26]; par-2(ok1723)</i>	This study	MOT661
Oligonucleotides		
Primer: <i>par-6(3' UTR) Forward:</i> GTAATACGACTCACTATAGGGCaaaa ctctttcagccattttcc	This paper	N/A
Primer: <i>par-6(3' UTR) Reverse:</i> GCGTAATACGACTCACTATAGGGC tcactaataatgtgaatttcagg	This paper	N/A
Recombinant DNA		
Feeding RNAi: <i>par-2</i>	Motegi et al., 2011	pFM63
Ahringer Feeding RNAi: <i>par-1</i>	Source BioScience	sjj_H39E23.1
Ahringer Feeding RNAi: <i>par-6</i>	Source BioScience	sjj_T26E3.3
Ahringer Feeding RNAi: <i>nos-3</i>	Source BioScience	sjj_Y53C12B.3
Ahringer Feeding RNAi: <i>lgl-1</i>	Source BioScience	sjj_F56F10.4
Ahringer Feeding RNAi: <i>chin-1</i>	Source BioScience	sjj_BE0003N10.2
Ahringer Feeding RNAi: <i>cdc-42</i>	Source BioScience	sjj_R07G3.1

(Continued on next page)

Continued

REAGENT or RESOURCE	SOURCE	IDENTIFIER
Software and algorithms		
Metamorph software	Intelligent Imaging Innovation	https://www.moleculardevices.com/ products/cellular-imaging-systems/ acquisition-and-analysis-software/ metamorph-microscopy
Fiji (ImageJ)	NIH	https://fiji.sc/
ImaEdge software for MATLAB	Zhang et al., 2017	https://github.com/KanchanawongLab/ ImaEdge
Prism 7.0	GraphPad	https://www.graphpad.com/ scientific-software/prism/

RESOURCE AVAILABILITY**Lead contact**

Requests for resources and further information should be directed and will be fulfilled by the lead contact (motegi@igm.hokudai.ac.jp).

Materials availability

All unique materials supporting the findings of this study are available from the Lead Contact with a completed Materials Transfer Agreement.

Data and code availability

The datasets supporting the current study have not been deposited in a public repository, but are available from the corresponding author on request. The source code of ImaEdge software can be downloaded from Github (<https://github.com/KanchanawongLab>).

EXPERIMENTAL MODEL AND SUBJECT DETAILS

C. elegans strains were reared on standard Nematode Growth Media (NGM) seeded with *Escherichia coli* strain OP50 or HT115 as food. All strains were maintained at 20°C and shifted to 25°C for 20–30 hours before recording. A list of strains used in this study is available in [Key resources table](#). Embryos were prepared from gravid hermaphrodite animals at early adult stage. Some strains listed below were sourced from the CGC, funded by NIH Office of Research Infrastructure Programs (P40 OD010440).

METHOD DETAILS**RNA interference (RNAi)**

RNAi experiments, except for *par-6(3'UTR RNAi)*, were performed by the feeding method. L4440-based RNAi clones were transformed into *E. coli* HT115 cells. The transformants were grown at 37°C in liquid LB media supplemented with 500 µg/mL carbenicillin. A volume of 100 µL of transformed *E. coli* liquid culture was seeded onto NGM plates with 1 mM IPTG, and incubated at room temperature overnight. Worms at the L3/L4 stage were transferred to feeding RNAi plates and incubated at 25°C for 24 hours. *par-6(3'UTR RNAi)* was performed by the soaking method. *par-6 3' UTR* sequence was prepared by PCR with primers listed in [Key resources table](#) and genomic DNA of N2 worms as a template. Double-stranded RNA (dsRNA) was prepared by *in vitro* transcription of a PCR product with T7 RNA polymerase. Worms at the L4 stage were incubated in a solution containing dsRNA at concentration 1 mg ml⁻¹ at 20°C for 24 hours, and then grown on an NGM plate at 25°C. Their phenotypes were observed 24 hours after removal of from the dsRNA solution.

Imaging of *C. elegans* embryos

Live imaging: *C. elegans* embryos were isolated from gravid hermaphrodite animals into egg salt buffer, placed on coverslips, and inverted on to slides with 20 µm monodisperse polystyrene beads (Bangs Laboratories, Inc.). Embryos were observed at 25°C with a CFI Plan Apochromat 60 × N.A.1.4 oil immersion lens on a Nikon Ni-E motorized upright microscope (Nikon) fitted with a CSU-X1 spinning disk confocal system (Yokogawa Electric Corp.) with LaserStack 491, 561, and 642 solid-state diode lasers (Intelligent Imaging Innovation Inc.). Images were acquired with a Photometrics Evolve512 camera (Photometrics) controlled by Metamorph software (Intelligent Imaging Innovation Inc.) using a 250 ms exposure at 20% power on the 491 and 561 lasers and 1 × 1 binning in the camera. Nuclear envelope breakdown (NEBD) was defined as the first frame when the GFP fusion was no longer excluded from pronuclei.

Immunofluorescence: Embryos were isolated into egg buffer and fixed on poly-lysine-coated slides using methanol at -20°C for 20 min, followed by acetone at -20°C for 10 min. The primary antibodies used were rabbit anti-PAR-2 (Hoege et al., 2010), rabbit anti-PAR-1 (Gönczy et al., 2001), rabbit anti-PKC-3 (Tabuse et al., 1998), mouse anti-PAR-3 (P4A1, DSHB), mouse anti-PGL-1 (K76, DSHB), and mouse anti-MEX-5 (Griffin et al., 2011; Schubert et al., 2000). Secondary antibodies used were goat anti-rabbit coupled to Alexa488, goat anti-rabbit coupled to Cy3, or goat anti-mouse coupled to Cy3 or Cy5, all at a 1:8,000 dilution. Samples were mounted with Vectashield Antifade Medium with DAPI (Vector Laboratories) to stain DNA.

Modeling of PAR polarity in zygotes

Previous models of PAR polarity in *C. elegans* zygotes

Previous models (Blanchoud et al., 2015; Dawes and Munro, 2011; Goehring et al., 2011) considered two species of PAR proteins. The anterior group of proteins (A) comprises of PAR-3, PAR-6, PKC-3, and CDC-42. The posterior group of proteins (P) is consisted of PAR-1, PAR-2, and LGL-1 (Figure S4A). The local cortical concentrations of A and P at time t and cortical position x, were designated by A and P , respectively, and were calculated from the following equations:

$$\begin{aligned} \frac{\partial A}{\partial t} &= D_A \frac{\partial^2 A}{\partial x^2} - \frac{\partial(vA)}{\partial x} + [K_{on,A} A^{cyto} - K_{off,A} A - K_{PA} P^\delta A] \\ \frac{\partial P}{\partial t} &= D_P \frac{\partial^2 P}{\partial x^2} - \frac{\partial(vP)}{\partial x} + [K_{on,P} P^{cyto} - K_{off,P} P - K_{PA} A^\delta P] \end{aligned}$$

D_A and D_P represent the diffusivity of each PAR species in the membrane-bound state. $v(x,t)$ refers to the cortical flow velocity. $K_{on,A}$, $K_{off,A}$, $K_{on,P}$, and $K_{off,P}$ are values for the respective coefficients for cortical association and dissociation of each PAR species. A^{cyto} and P^{cyto} are uniform cytoplasmic concentrations of A and P proteins, respectively. The second terms on the right side describe the initial segregation of both PAR species, which is mediated by advective cortical flow from the posterior pole to the anterior pole.

The above-described models (Blanchoud et al., 2015; Dawes and Munro, 2011; Goehring et al., 2011) reproduced the establishment and the maintenance of the steady-state PAR species distribution in wild-type zygotes. The model by Goehring et al. (2011) also reproduced the PAR patterns in *spd-5(RNAi)* zygotes where advective cortical flows were attenuated. It also recapitulated the shift of a boundary position between two cortical domains in zygotes where either A or P was overexpressed or knocked-down (Goehring et al., 2011). However, these models were unable to reproduce the PAR distributions in zygotes wherein PAR-2 was predominant (by a combination of GFP::PAR-2 overexpression and *par-6(pRNAi)* treatment) (Figure S4C).

A revised model of PAR polarity in *C. elegans* zygotes

To explain our observations and include findings from recent literatures, we revised the previous models by incorporating two additional PAR species, [CDC-42-PAR-6-PKC-3] and [CHIN-1], and including several molecular interactions among them (Figures 3A and S4B). PAR-3 recruits PAR-6 and PKC-3 to cortical cluster structures during polarization (Wang et al., 2017). CDC-42 can recruit PAR-6 and PKC-3 to the cortex independently of PAR-3 clusters (Rodriguez et al., 2017; Wang et al., 2017). Hence, the anterior cortical domain contains at least two species, [PAR-3-PAR-6-PKC-3] and [CDC-42-PAR-6-PKC-3]. CHIN-1 has been shown to localize at the posterior cortex and restricts activation of CDC-42 at the anterior cortical domain (Kumfer et al., 2010; Sailer et al., 2015). PAR-2 is essential to recruit PAR-1 (Boyd et al., 1996) but dispensable to localize CHIN-1 at the posterior cortex (Sailer et al., 2015). CHIN-1 and PAR-1-PAR-2 act in parallel to maintain the polarized PAR domains (Sailer et al., 2015). Thus, the posterior cortical domain includes at least two species, [CHIN-1] and [PAR-1-PAR-2]. We did not include another posterior protein, LGL-1, because it is dispensable to pattern the cortical PAR domains (Beatty et al., 2010; Hoege et al., 2010). Hence, our revised model for the establishment of PAR polarity relies on four species of PAR proteins. [CDC-42-PAR-6-PKC-3] and [PAR-3-PAR-6-PKC-3] are referred as A_1 and A_2 , respectively, as they localize at the anterior cortical domain. [CHIN-1] and [PAR-1-PAR-2] are referred as P_1 and P_2 , respectively, as they localize at the posterior cortical domain.

A_1 : CDC-42-PAR-6-PKC-3

A_2 : PAR-3-PAR-6-PKC-3

P_1 : CHIN-1

P_2 : PAR-1-PAR-2

Given that CDC-42 is essential for PKC-3 to exclude PAR-2 independently of PAR-3 (Rodriguez et al., 2017), we included an inhibitory interaction from A_1 [CDC-42-PAR-6-PKC-3] to P_2 [PAR-1-PAR-2] in our model. Two previous reports (Rodriguez et al., 2017; Wang et al., 2017) also proposed that PAR-6 and PKC-3 could associate with either PAR-3 or CDC-42 on the cortex. Because PAR-3 is generally essential to recruit PAR-6 and PKC-3 during polarization (Wang et al., 2017), we include a positive interaction from A_2 [PAR-3-PAR-6-PKC-3] to A_1 [CDC-42-PAR-6-PKC-3]. CHIN-1 is excluded from the anterior cortex through an unknown mechanism that relies on PKC-3 (Sailer et al., 2015), and interferes active CDC-42 within the posterior cortical domain (Kumfer et al., 2010; Sailer et al., 2015). We thus include reciprocal inhibitory interactions: one from A_1 [CDC-42-PAR-6-PKC-3] to P_1 [CHIN-1], the other from P_1 [CHIN-1] to A_1 [CDC-42-PAR-6-PKC-3].

Diffusion rates of all four species in the cytoplasm are assumed to be much faster than their respective rates on the cell cortex (Goehring et al., 2011). Therefore, cytoplasmic concentration of these species should be uniform and quasi-statically adapted to their

molecular interactions on the cortex. We denoted the cortical concentration of four species as A_1 , A_2 , P_1 , and P_2 , the time evolution of the local concentration on the membrane at time t and position x is described by the following equations:

$$\begin{aligned}\frac{\partial A_1}{\partial t} &= D_{A1} \frac{\partial^2 A_1}{\partial x^2} + [K_{on,A_1}(1 + K_{A_1 A_2} A_2^\gamma) A_1^{cyto} - K_{off,A_1} A_1 - K_{A_1 P_1} P_1^\alpha A_1] \\ \frac{\partial P_1}{\partial t} &= D_{P1} \frac{\partial^2 P_1}{\partial x^2} + [K_{on,P_1} P_1^{cyto} - K_{off,P_1} P_1 - K_{P_1 A_1} A_1^\beta P_1] \\ \frac{\partial A_2}{\partial t} &= D_{A2} \frac{\partial^2 A_2}{\partial x^2} + [K_{on,A_2} A_2^{cyto} - K_{off,A_2} A_2 - K_{A_2 P_2} P_2^\delta A_2] \\ \frac{\partial P_2}{\partial t} &= D_{P2} \frac{\partial^2 P_2}{\partial x^2} + [K_{on,P_2} P_2^{cyto} - K_{off,P_2} P_2 - K_{P_2 A_1} A_1^\zeta P_2]\end{aligned}\quad \text{Equation 1}$$

On the right side, the first terms are diffusion terms describing diffusional transport on the cortex with diffusion constants, D_{A_1} , D_{P_1} , D_{A_2} , and D_{P_2} . The next three terms are reaction terms explaining molecular interactions among the PAR species. The second set of terms describe cortical binding with binding rates K_{on,A_1} , K_{on,P_1} , K_{on,A_2} , and K_{on,P_2} per unit cytosolic concentrations. For example, in the first equation, the binding of A_1 is promoted by the presence of A_2 with the coefficient $K_{A_1 A_2}$. The third set of terms explain dissociation rates from the cortex with the unbinding rates K_{off,A_1} , K_{off,P_1} , K_{off,A_2} , and K_{off,P_2} . The fourth set of terms also refer to dissociation stimulated by the mutual antagonism between the molecules P_1 and A_1 with the rates $K_{A_1 P_1}$ and $K_{P_1 A_1}$, the inhibition from P_2 to A_2 with the rate $K_{A_2 P_2}$, and the inhibition from A_1 to P_2 with the rate $K_{P_2 A_1}$. Cytosolic concentrations of each PAR species were calculated from total concentration minus cortical concentration. For example, cytosolic concentrations of A_1 can be described as following:

$$A_1^{cyto} = A_1^{\text{total}} - \psi \overline{A_1}; \overline{A_1} = \frac{1}{L} \int_{-\frac{L}{2}}^{\frac{L}{2}} A_1 dx,$$

ψ is the surface-to-volume conversion factor. L is the perimeter along the anteroposterior axis of zygote (Goehring et al., 2011). Since the periphery of the zygote was assumed to be a one-dimensional space, Equation 1 was considered under the periodic boundary condition. We used MATLAB to obtain numerical values of steady-state solutions in Equation 1. For the initial condition, we considered a spatially uniform steady-state solution for the four variables and put higher values for P_1 and P_2 in the posterior region. Depending on the parameter sets, various PAR species (A_1 , P_1 , A_2 , and P_2) can distribute either uniformly or asymmetrically in a specific region of the cortex.

Like the previous models (Blanchoud et al., 2015; Dawes and Munro, 2011; Goehring et al., 2011), our model also requires multi-stability in the reaction terms that allows each PAR species to account for both the unpolarized and the polarized state at the cortex. Given that our modeling did not consider the advection term and relied on both the diffusion term and the reaction term, our simulation only constructs the steady-state distribution of each PAR species in zygotes.

The steady-state concentration profiles in wild-type (WT) condition are shown in Figure 3B. A_1 [CDC-42-PAR-6-PKC-3] and A_2 [PAR-3-PAR-6-PKC3] are enriched in the anterior domain, whereas the posterior domain shows high concentrations of P_1 [CHIN-1] and P_2 [PAR-1-PAR-2]. Hereafter, we normalized concentrations (A_1 , A_2) and (P_1 , P_2) with A_{max} and P_{max} , respectively. A_{max} and P_{max} are the maximum values of cortical concentration in A_1 and A_2 , and in P_1 and P_2 , respectively. We then plotted normalized concentrations of the respective proteins against the length of the embryo, from the anterior to the posterior poles. The cortical domain size of each PAR species is defined as the percentage of the cortical region where protein concentration is equal to or greater than 40% of its maximum concentration at the cortex. The domain size of A_1 species, for example, can be calculated by using the following formula:

$$\text{domain size} = \frac{\int \delta[A_1(x) - 0.4 \times A_{1max}] dx}{\oint dx}$$

where the cortical concentration of A_1 at the cortical position x is defined as $A_1(x)$, $\delta[x]$ is the Heaviside step function, and $\oint dx = L$.

The parameter values we used for simulation of WT zygotes and zygotes wherein the levels of one (or more) PAR species were modified are summarized in Table S1. To conduct a robustness assessment of the parameter values that had not been defined by *in vivo* measurement, we applied perturbations to individual parameter space ranging from 50% to 200% of the original value in Table S4 and simulated the pattern of cortical domains with the combinatorial PAR network model. This analysis revealed that the polar pattern is maintained in the 50%–200% range for all unknown parameters (K_{on,A_2} , K_{on,P_1} , K_{off,A_2} , K_{off,P_1} , D_{A_2} , D_{P_1} , $K_{P_1 A_1}$, and $K_{A_2 P_2}$) (Figure S4H). Although there are some variations in the size of the cortical domains, the bipolar pattern of cortical PAR domains is generally insensitive to such changes in these parameter values. Among the parameters we tested, the cortical PAR domain sizes are relatively sensitive to a fluctuation in the total concentration of A_1 .

To simulate experimental conditions where one (or more) PAR species was either knocked-down (KD), knocked-out (KO), or over-expressed (OE), we changed total concentrations of each PAR species in our simulations as they would have experimentally. The results for *in silico* KD, KO, OE manipulations are explained in detail below, and are shown in Figures 3C–3I and S4D–S4G.

PAR polarity in either PAR-6 KO and PAR-2 KO conditions

When the total concentration of A_1 (A_1^{total}) or P_2 (P_2^{total}) is at zero, cortical polarity exhibits nearly uniform distribution of P_2 or A_1 , respectively (Figures 3C and 3D). These results are consistent with previous observations (Boyd et al., 1996; Cuenca et al., 2003; Hung and Kemphues, 1999) and our results in Figure 1B.

PAR polarity in PAR-2 KD and PAR-2 OE conditions

When P_2^{total} is reduced from the WT value of 1 to 0.1, the size of cortical P_2 domain decreased, and that of cortical A_1 domain increased, shifting the boundary between the A_1 and the P_2 domains from anterior to posterior (Figures 3F and S4D). When the total concentration of P_2 (P_2^{total}) is increased from the WT value of 1 to 5, the size of cortical P_2 domain increased, and that of cortical A_1 domain reduced, shifting the boundary between the A_1 and the P_2 domains from posterior to anterior (Figures S4D and S4E). These results are consistent with the previous observation (Goehring et al., 2011) and our results in Figure 1A.

PAR polarity in PAR-2 OE at WT and PAR-6 KD background conditions

To systematically explore the effect of different levels of PAR-2 OE *in silico*, the total concentration of P_2 (P_2^{total}) is increased from the WT value of 1 to 10. The corresponding size of A_1 and P_2 domains are shown in Figures S4D and S4E. The changes in cortical domain sizes in response to PAR-2 OE exhibit two distinct phases: When P_2^{total} increases from 1, the size of A_1 domain gradually decreases due to the expansion of P_2 domain. At around $P_2^{\text{total}} = 15$, the solution of Equation 1 shows a bifurcation, leading to a qualitative change in the distribution of concentrations. At this bifurcation point, distribution of P_2 changes from the polarized state to the unpolarized state showing high concentration of P_2 throughout the cortex. Despite the P_2 distribution throughout the cortex, the distribution of A_1 remains at the polarized state (Figures S4D and S4E).

We next tested if PAR-6 KD could compromise the stability of the polarized state of PAR-2 in response to PAR-2 OE treatment. When A_1^{total} is lower than the WT value, the increase in P_2^{total} causes a similar bifurcation for P_2 (the distribution changes from the polarized state to the unpolarized state) at a lower value of P_2^{total} compared to the WT case (Figures 3H and S4F). Such a shift of the bifurcation point in P_2^{total} can be explained by the antagonistic interaction from A_1 to P_2 . Because A_1 antagonizes P_2 , a lower level of A_1^{total} permits P_2 to dominate the entire cortex even at lower P_2^{total} . This result is consistent with our observation of *par-6(pRNAi)* zygotes overexpressing GFP::PAR-2 in Figure 1A.

PAR polarity in CHIN-1 KD conditions with or without PAR-2 OE

At the WT background, a reduction in P_1^{total} does not cause significant changes in the distribution patterns in A_1 , A_2 , and P_2 (Figure 3E). In contrast, under P_2 OE condition, reduction in P_1^{total} depolarizes A_1 domain at the P_2 bifurcation point where P_2 becomes uniform at the cortex (Figures 3I and S4G). This result suggested a role of CHIN-1 in maintaining cortical PAR-6 domain in zygotes with a PAR-2 predominance. This is consistent with our observation of *chin-1(RNAi);par-6(pRNAi)* zygotes overexpressing GFP::PAR-2 in Figure 2F.

Modeling of PAR polarity in two-cell-stage embryos

To simulate the distribution of PAR proteins in two-cell-stage embryos, we applied the cross-inhibitory network involving the four PAR species (A_1 , A_2 , P_1 , and P_2) in Equation 1, which was used for the PAR pattern simulation in zygotes, to AB and P1 cells. We considered simulation data of the steady-state distribution of the PAR species in zygote for the initial condition of two-cell-stage embryos. The PAR species were then compartmentalized between AB and P1 cells at the position of a cleavage furrow, which was experimentally measured in zygotes. Therefore, the initial profile of the PAR species in AB and P1 cells were copied respectively from the anterior and posterior portion of the zygote with length L_{AB} and L_{P1} ($L_{AB} + L_{P1} = L$, the total perimeter of the zygote). Based on *in vivo* observations, we set $L_{AB} = 0.55 \times L$ and $L_{P1} = 0.45 \times L$ for both wild-type and PAR-2-predominant embryos and $L_{AB} = L_{P1} = 0.50 \times L$ for *cye-1(RNAi)* embryos.

PAR polarity in wild-type embryos

Through unequal inheritance of all four PAR species during the first cell division, AB and P1 cells inherited different total concentration of the PAR species. The AB cell increased the total concentration of A_1 and A_2 and decreased the total concentration of P_1 and P_2 . The total concentration of the PAR species in the P1 cell were determined according to the law of mass conservation. Therefore, the P1 cell decreased the total concentration of A_1 and A_2 and increased the total concentration of P_1 and P_2 . For the zygote and its daughter cells, the law of mass conservation was given as

$$C_0 \times V_0 = C_1 \times V_1 + C_2 \times V_2$$

where C_0 , C_1 , and C_2 are the total PAR concentration (A_1^{total} , A_2^{total} , P_1^{total} , or P_2^{total}) in zygote, AB cell, and P1 cell, respectively. V_0 , V_1 , and V_2 are their respective volumes. For the wild-type conditions, $V_1/V_0 = 0.55$ and $V_2/V_0 = 0.45$. With the given changes in the total concentration of A_1 , A_2 , P_1 and P_2 , the distribution of the PAR species in AB and P1 cells were numerically calculated until their spatial pattern reached the steady state. Simulations in other conditions, such as PAR-2 overexpression (P2OE) and *cye-1(RNAi)* with higher or lower levels of PAR-2, were performed in a similar approach. The particular changes from simulations in the wild-type condition are summarized below.

PAR polarity in P2OE embryos

A higher total concentration of P_2 was used for simulation of the steady state in zygotes. Because of nearly symmetric distribution of A_2 and P_2 in the P2OE zygotes, the total concentration of A_2 and P_2 in AB and P1 cells were similar to those in the zygote. The total

concentration of A_1 was increased and that of P_1 was decreased for the AB cell, while the total concentration of A_1 was decreased and that of P_1 was increased for the P1 cell, satisfying the conservation law. The parameter values are summarized in [Table S2](#).

PAR polarity in *cye-1(RNAi)* embryos

Because of equal inheritance of all PAR proteins between the *cye-1(RNAi)* daughter cells, the total concentrations of A_1 , A_2 , P_1 , and P_2 in these cells were the same as those in the zygote. For the initial condition of the daughter cells, we considered a spatially uniform steady state solution for the four variables (A_1 , A_2 , P_1 , and P_2) with random fluctuations. The total concentration of P_2 was modified to simulate the cells with higher or lower P_2 condition. The parameter values are summarized in [Table S3](#).

QUANTIFICATION AND STATISTICAL ANALYSIS

Quantification of PAR proteins and fate determinants

To quantify the distribution of PAR proteins at the cell cortex in live zygotes ([Figure S2](#)), we used ImaEdge software ([Zhang et al., 2017](#)), which was designed for automatic extraction of the cortex region from each frame of time-lapse movies. The cortical region along the entire circumference was divided into 100 sampling windows. The maximum intensity in each sampling window was used to represent the amount of proteins-of-interest at the cortex. We then generated a 2D heatmap with the frame number as the horizontal axis and the position of the sampling windows as the vertical axis to integrate the spatiotemporal information of cortical PAR proteins.

The total levels of GFP::PAR-2 in zygotes were estimated by the average fluorescence intensities of GFP::PAR-2 in the cytoplasm of zygotes shortly after fertilization (before polarization of GFP::PAR-2 at the cortex). A box of $75.1 \mu\text{m}^2$ at the center position in the GFP::PAR-2 images (taken at about $2 \mu\text{m}$ below the upper lateral cortex) was used to measure the average intensity. The GFP::PAR-2 intensity of each zygote was normalized to the mean value of GFP::PAR-2 intensity in embryos expressing unmodified *gfp::par-2* transgene (JH2952).

The sizes of cortical GFP::PAR-2 and mCherry::PAR-6 domains were determined by the extent of each fluorescence protein occupying the circumference of the zygote. The surface of the zygote was manually traced using ImageJ software. The edge of each cortical domain was defined at the region where either GFP::PAR-2 or mCherry::PAR-6 intensity is about 40% of the maximum intensity within the corresponding cortical domain. The length of the cortical PAR-2 domain and that of the cortical PAR-6 domain were independently measured and represented as a percentage of the total circumference of the zygote.

The distribution of cortical PAR proteins (PAR-1, GFP::PAR-2, PAR-3, and mCherry::PAR-6) in zygotes were assessed by the integrated intensity of cortical PAR proteins within the anterior and the posterior cortical domains. The surface of the zygote was manually traced and divided into two halves with Metamorph software using the line-scan function. The segregation of the posterior proteins (PAR-1 and GFP::PAR-2) was represented as a ratio of their average intensity within the posterior domain to that within the anterior domain. The segregation of the anterior proteins (PAR-3 and mCherry::PAR-6) was represented as a ratio of their average intensity within the anterior domain to that within the posterior domain.

The distribution of cytoplasmic fate determinants (MEX-5 and PIE-1) were assessed by their average intensity within the anteromedial and the posteromedial cytoplasm, respectively. A box of $75.1 \mu\text{m}^2$ or $27.0 \mu\text{m}^2$ was used to measure the intensities of MEX-5 and PIE-1, respectively, with Metamorph software. The segregation of MEX-5 was represented as a ratio of the average intensity within the anteromedial cytoplasm over that within the posteromedial cytoplasm. The segregation of PIE-1 was represented as a ratio of the average intensity within the posteromedial cytoplasm over that within the anteromedial cytoplasm.

Statistical tests and reproducibility

All statistical tests were performed using GraphPad Prism 7.0. All results presented in graphs represent the mean \pm s.d. The D'Agostino-Pearson omnibus test was used for normality testing. A Student's t test (two-tailed distribution) and non-parametric Mann-Whitney U-test were used to calculate p values. The exact sample number value (the number of embryos) is indicated in the corresponding figure and figure legend. All experiments with or without quantification were independently repeated at least three times with similar results, and the representative data are shown. Animals were randomly distributed among the different conditions, since the animals did not exhibit any appearance differences. No animals and embryos were excluded for the data analysis. No statistical method was used to predetermine the sample size. The experiments were not randomized. The investigators were not blinded to allocation during experiments or outcome assessment.